RSC Advances

ROYAL SOCIETY OF CHEMISTRY

www.rsc.org/advances

Journal Name

ARTICLE

On the Constitution and Thermodynamic Modelling of the System Ti-Ni-Sn

Received 00th January 20xx,
Accepted 00th January 20xx

DOI: 10.1039/x0xx00000x

www.rsc.org/

M. Gürth,[abc] A. Grytsiv,[abc] J. Vrestal[d], V.V. Romaka[e], G. Giester[f], E. Bauer[bc] and P. Rogl[ab]

Phase equilibria of the system Ti-Ni-Sn have been determined for the isothermal section at 950°C based on X-ray powder diffraction (XPD) and electron probe microanalysis (EPMA) of about 60 ternary alloys in as cast and annealed state. The section is characterized by the formation of four ternary compounds labelled τ_1 to τ_4. Whereas two of the ternary compounds are found without significant homogeneity regions: τ_1-TiNiSn (Half Heusler phase, MgAgAs-type), τ_3-Ti_2Ni_2Sn (U_2Pt_2Sn-type), τ_4-$(Ti_{1-x-y}Sn_xNi_y)Ni_3$ with $AuCu_3$-type exhibits a solution range ($0.22 \le x \le 0.66$ and $0.22 \ge y \ge 0.02$) and a particularly large homogeneity region is recorded for τ_2-$Ti_{1+y}Ni_{2-x}Sn_{1-y}$ (Heusler phase, $MnCu_2Al$-type). Extended solid solutions starting from binary phases at 950°C have been evaluated for $Ti_5Ni_{1-x}Sn_3$ (filled Mn_5Si_3 = Ti_5Ga_4-type; $0 \le x \le 1$), $Ti_{1-x}Sn_xNi_3$ ($TiNi_3$-type; $0 \le x \le 0.27$) and $(Ti_{1-x}Ni_x)_{1-y}Sn_y$ (CsCl-type) reaching a maximum solubility at x=0.53, y=0.06). From differential thermal analysis (DTA) in alumina crucibles under argon a complete liquidus surface has been elucidated revealing congruent melting for τ_2-$TiNi_2Sn$ at 1447°C, but incongruent melting for τ_1-TiNiSn (pseudobinary peritectic formation: $\ell + \tau_2 \leftrightarrow \tau_1$ at 1180°C), τ_3-Ti_2Ni_2Sn (peritectic formation: $L + \tau_2 + Ti_5NiSn_3 \leftrightarrow \tau_3$ at 1151°C) and τ_4-$Ti_{1-x}Sn_xNi_3$ (peritectic formation: $L+TiNi_3+(Ni) \leftrightarrow \tau_4$). A Schultz-Scheil diagram for the solidification behavior was constructed for the entire diagram involving 20 isothermal four-phase reactions in the ternary. For a thermodynamic CALPHAD assessment of the ternary diagram we relied on the binary boundary systems as modelled in the literature. As thermodynamic data in the ternary system were only available in the literature for the compounds $TiNi_2Sn$ and TiNiSn, heat of formation data were supplied by our density functional theory (DFT) calculations for Ti_2Ni_2Sn, as well as for the solid solutions, which were modelled for $Ti_{1-x}Sn_xNi_3$, $Ti_5Ni_{1-x}Sn_3$ and $(Ti_{1-x}Ni_x)_{1-y}Sn_y$. Thermodynamic calculation was performed with the Pandat software and finally showed a reasonably good agreement for all the 20 invariant reaction isotherms involving the liquid.

1 Introduction

The so-called "Half Heusler" (HH) compound TiNiSn, known as an n-type semiconductor since 1986 [1,2], has hitherto displayed a high potential for exceptional efficiency in thermoelectric (TE) generators converting (waste) heat into electricity. Thermoelectric research has, therefore, focused mainly on improvement of ternary intermetallic compounds based on TiNiSn, which crystallize with the non-centrosymmetric cubic MgAgAs-type structure (space group $F\bar{4}3m$). Beside skutterudites and clathrates, HH compounds are promising candidates for high temperature thermoelectric applications because they inherit a tuneable electronic structure, which can be modified through (i) doping/substitution on its three metal sublattices, (ii) engineering of a generally narrow band gap, and (iii) nanostructuring via ball-milling and precipitation of secondary system inherent phases as the most prominent among many other techniques. An overview on the thermoelectric properties of HH alloys, reaching up to 700°C a ZT_{max}~1.0 for p-type $Ti\{Fe_xCo_{1-x}\}\{Sn_ySb_{1-y}\}$ and a ZT_{max}~1.2 for n-type $\{Ti_{1-u-v}Zr_uHf_v\}Ni\{Sn_{1-w}Sb_w\}$ can be found from a recent review article. [3] However, the biggest disadvantage of HH alloys is their relatively high thermal conductivity, which has to be decreased in order to increase the thermoelectric performance of these materials. Large scale production and particularly nanostructuring of TE-materials by precipitation of preferably system inherent phases, however, needs a profound knowledge not only of isothermal phase relations, temperature dependent solubilities and vacancy concentrations but also of the solidification behaviour in each ternary subsystem of any multi-component TiNiSn-based alloy

[a] Institute of Material Chemistry and Research, University of Vienna, Währingerstrasse 42, A-1090 Wien, Austria.
[b] Christian Doppler Laboratory for Thermoelectricity, Wien, Austria.
[c] Institute of Solid State Physics, TU-Wien, Wiedner Hauptstrasse, 8-10, A-1040 Wien, Austria.
[d] Masaryk University, CEITEC, Kamenice 753/5, Brno, Czech Republic.
[e] Department of Materials Science and Engineering, Lviv Polytechnic National University, 79013 Lviv, Ustiyanovycha Str. 5, Ukraine.
[f] Institute of Mineralogy and Crystallography, University of Vienna, Althanstrasse 14, A-1090 Wien, Austria.
Corresponding author: Peter Rogl; e-mail: peter.franz.rogl@univie.ac.at
†Electronic Supplementary Information (ESI) available: [Tables S1, S2, S3]. See DOI: 10.1039/x0xx00000x

system. Although several papers in the literature provide (a) phase relations in the isothermal section of Ti-Ni-Sn at 800°C [4] (see also refs. therein), (b) melting temperatures of TiNiSn (T_m=1182°C [5]; T_m=1182°C [6]), $TiNi_2Sn$ (T_m=1447°C [5]), (c) DFT heat of formation data for various binary and ternary compounds,[5,7] (d) calorimetric heat of formation data [8] and (e) coefficient of thermal expansion $\alpha_{ave}=11.3\times10^{-6}$ K^{-1} (40° - 690 °C) [6], to our best knowledge hitherto no liquidus projection exists. For most reports in the literature the homogeneity regions of the Heusler and the Half Heusler phase play no important role, but several authors gave proof to the non-stoichiometry of $TiNi_{2-y}Sn$ (0<y<0.04, 800°C [4]; 0<y<0.22, as cast [5]) and of $TiNi_{1+y}Sn$ (0<y<0.10, as cast [5]; 0<y<0.06, 900°C [9]; -0.06<y<0.08, at 1100°C [10]).

In order to shed light on the complicated synthesis procedures for single-phase TiNiSn-based alloys, the present paper is intended to provide (1) a liquidus surface for the entire Ti-Ni-Sn phase diagram i.e. precise information on the solidification paths, and (2) phase relations in an isothermal section at 950°C. As the TiNiSn system is a subsystem of a multi component thermoelectric alloy system, for which a thermodynamic (pre-) calculation can save extensive experimental work, the present paper will furthermore provide a thermodynamic assessment of the Ti-Ni-Sn ternary. This CALPHAD-type modelling is based on existing assessments for the binary boundary systems as well as relies on experimental thermodynamic data for the ternary compounds and will be backed by DFT energies of formation wherever needed in the modelling.

2 Experimental details

2.1. Sample preparation and characterization.

Pure elements in form of Ti-, Ni-rods, Sn-shot or bars with a minimum purity of 99.95 mass% from Alfa Aesar were used for the preparation of about 60 alloys with various compositions for the system TiNiSn. First stoichiometric amounts of Ti and Ni were arc melted together under 6N Argon and then the proper amount of Sn was added. The reguli were flipped 3 times for a better homogenization. Afterwards the samples were vacuum sealed in quartz ampullae (which were backfilled at RT with 200 mbar Ar), annealed at different temperatures for 7 days (200°C→950°C with a heating rate of 10°C/min) and water quenched. Some samples were further annealed in evacuated quartz ampullae (which were backfilled at RT with 200 mbar Ar) at different temperatures in Al_2O_3 crucibles for better equilibration.

For sample characterization we used Scanning Electron Microscopy (SEM), Electron Probe Microanalysis (EPMA) and X-ray Powder Diffraction (XPD). The microstructure and chemical composition of the alloys were analyzed by SEM on a Zeiss Supra 55 VP equipped with an energy dispersive X-ray (EDX) detector operated at 20 kV. Samples for EPMA were prepared by standard metallographic methods. In some cases polishing was performed under glycerine instead of water to avoid oxidation and/or hydrolysis of samples. X-ray powder diffraction profiles for all alloys were collected from a HUBER-Guinier image plate with monochromated $CuK_{\alpha1}$-radiation. For Rietveld refinements we used the FullProf program [11], whilst precise lattice parameters were obtained by least square methods with program STRUKTUR [12] employing pure Ge (99.9999%) as internal standard (a_{Ge} = 0.5657906 nm).

Single crystals of Ti_5NiSn_3 were isolated from alloy $Ti_{53}Ni_{11}Sn_{34}$ annealed at 1100°C for 5 days. The crystals were inspected on an AXS-GADDS texture goniometer for quality and crystal symmetry prior to X-ray single crystal (XSC) intensity data collection on a four-circle Nonius Kappa diffractometer (CCD area detector and graphite monochromated MoK_α radiation, λ = 0.071069 nm). Orientation matrix and unit cell parameters were derived using the program DENZO (Nonius Kappa CCD, Program Package, Nonius Delft, The Netherlands). Besides psi-scans no additional absorption correction was necessary because of the rather regular crystal shape and small dimensions of the investigated specimens. The structure was solved by direct methods and refined with the SHELXS-97 and SHELXL-97 programs [13], respectively.

The differential thermal analyses (DTA) measurements were performed on annealed samples in a Netzsch 404 Pegasus DSC (differential scanning calorimetry) equipment in Al_2O_3-crucibles under a stream of 6N argon and a heating rate of 5 K/min. The equipment was calibrated in the temperature range from 300 to 1400°C against pure metal standards supplied by Netzsch to be within ±1°C.

2.2. Thermodynamic modelling

2.2.1. First-principles calculations.

The DFT calculations were carried out using the Elk v2.3.22 package [14] – an all-electron full-potential linearised augmented-plane wave (FP-LAPW) code with Perdew-Burke-Enzerhoff exchange-correlation functional in generalized gradient approximation (GGA) [15]. The APW basis set cut-off used in the calculations was set to 190 eV, and the *k*-grid was equal or higher than 10×10×10 *k*-points depending on the structure. Prior to final total energy calculations the geometry of the initial structures (lattice vectors and atomic coordinates) was completely relaxed. The proper values of the muffin-tin radii were selected automatically at the initial stage of the calculations. In general the enthalpy of formation (ΔH *in* (meV/atom)) at T = 0 K for a specific compound was calculated according to the following formula:

$$\Delta H=10^3[E_{tot}(Ti_aNi_bSn_c)-a(E_{tot}(Ti)/j)-b(E_{tot}(Ni)/k)-c(E_{tot}(Sn)/l)]/(a+b+c),$$

where *a*, *b*, *c* are the number of each type of atoms in the crystal lattice of compound used in calculations; *j*, *k*, *l* are the number of atoms in the crystal lattice of Ti, Ni, and Sn, respectively, used in the calculations; E_{tot} is the total energy of compound in eV.

2.2.2. CALPHAD modelling.

For thermodynamic and phase diagram calculations as well as for optimization of thermodynamic parameters based on the CALPHAD method, the Pandat software package [16] was used. Thermodynamic modelling of phases existing in this ternary

system relied on the well-known Compound Energy Formalism (CEF) [17] enabling us to respect the real crystallographic structure of a phase by means of a sublattice description. As fixed values we used thermodynamic data from existing thermodynamic assessments for the respective binary sub-systems as well as energy of formation data for the end-members of intermetallic phases at 0 K (data from DFT-calculations of the ground state energies for binary compounds).

For the thermodynamic description of the respective phase structures, commonly used thermodynamic models were applied with respect to reference Gibbs energies of components in given phase ϕ, which have a polynomial form [18]:

$$ {}^{0}G_i^{\phi}(T) = G_i^{\phi}(T) - {}^{0}H_i^{SER}(298.15K) = A + BT + CT\ln T + \sum_{n=2}^{\eta} D_n T^n \quad (1) $$

where A, B, C, D_n and n (typically equal to 2, 3, and -1) are constants characteristic for the particular structure of the element i in a given temperature interval in Kelvin. The reference Gibbs energy is defined relative to the molar enthalpy of the element ${}^{0}H_i^{SER}$ at 298 K and 1 bar in its Standard Element Reference state (SER).

The Gibbs energy of a given phase like liquid and solid solution or a compound is expressed as a sum of several contributions:

$$ G_m^{\phi} - \sum_{i=Ti,Ni,Sn} x_i \, {}^{0}H_i^{SER}(298.15) = {}^{ref}G_m^{\phi} + {}^{id}G_m^{\phi} + {}^{ex}G_m^{\phi} + {}^{ext}G_m^{\phi} \quad (2) $$

where ${}^{ref}G^{\phi}_m$ is the reference level of the molar Gibbs energy of a given phase ϕ, ${}^{id}G^{\phi}_m$ describes the ideal mixing of components and ${}^{ex}G^{\phi}_m$ is the excess Gibbs energy describing a non-ideal behavior of components due to their mutual interactions. The last external term ${}^{ext}G^{\phi}_m$, which includes other additional contributions to the overall Gibbs energy like e.g. pressure or surface contributions has not been used in the thermodynamic modelling of the Ti-Ni-Sn system with exception of magnetic contributions.

The particular terms in case of solution phases like liquid or solid solutions are described as follows:

$$ {}^{ref}G_m^{\phi} = \sum_{i=Ti,Ni,Sn} x_i \left(G_{m,i}^{\phi} - {}^{0}H_{m,i}^{SER}(298.15K) \right) \quad (3a) $$

$$ {}^{id}G_m^{\phi} = RT \sum_{i=Ti,Ni,Sn} x_i \ln x_i \quad (3b) $$

$$ {}^{ex}G_m^{\phi} = \sum_i \sum_{j>i} x_i x_j \, L_{i,j}^{\phi} + \sum_i \sum_{j>i} \sum_{k>j} x_i x_j x_k \, L_{i,j,k}^{\phi} \quad (3c) $$

with

$$ L_{i,j}^{\phi} = \sum_{n=0}^{s} {}^{n}L_{i,j}^{\phi} (x_j - x_i)^n \quad (3d) $$

$$ L_{i,j,k}^{\phi} = {}^{0}L_{i,j,k}^{\phi} \, x_i + {}^{1}L_{i,j,k}^{\phi} \, x_j + {}^{2}L_{i,j,k}^{\phi} \, x_k \quad (3e) $$

and

$$ {}^{n}L_{i,j}^{\phi} = a_n + b_n T + c_n T \ln T \quad (3f) $$

where x_i, x_j and x_k are molar fractions of elements i, j and k (Ti,Ni,Sn), respectively in the given phase and L are thermodynamic interaction parameters, allowing to express the excess Gibbs energy. The expressions (3d-f) introduce the generally used Redlich-Kister-Muggianu method [19,20] for evaluation of thermodynamic non-idealities in a binary and ternary phase.

Thermodynamic modelling of intermetallic phases is based on the compound energy formalism in which the particular terms are described as follows:

$$ {}^{ref}G_m^{\phi} = \sum_i \sum_j y_i' y_j'' \left(G_{i:j}^{\phi} - {}^{0}H_i^{SER}(298.15K) - {}^{0}H_j^{SER}(298.15K) \right) \quad (4a) $$

$$ {}^{id}G^{\phi} = RT\left(\nu_i' \sum_i y_i' \ln y_i' + \nu_i'' \sum_i y_i'' \ln y_i'' \right) \quad (4b) $$

$$ \begin{aligned} {}^{ex}G^{\phi} = & \sum_i \sum_{j>i} y_i' y_j' \sum_k y_k'' L_{i,j:k} + \sum_i \sum_{j>i} y_i'' y_j'' \sum_k y_k' L_{k:i,j} \\ & + \sum_i \sum_{j>i} \sum_k \sum_{l>k} y_i' y_j' y_k'' y_l'' L_{i,j:k,l} + \sum_i \sum_{j>i} \sum_{k>j} \sum_l y_i' y_j' y_k' y_l'' L_{i,j,k:l} \\ & + \sum_i \sum_{j>i} \sum_{k>j} \sum_l y_i' y_i'' y_j'' y_k'' L_{i:i,j,k} \end{aligned} \quad (4c) $$

where y_i is the site fraction of element i in the first or second sublattice (y_i' or y_i'') and ν_i is the stoichiometric coefficient of element i of the real or hypothetical compound and hence its stoichimetric ratio in the first or second sublattice (ν_i' or ν_i''). The meaning of other expressions is the same as above, but in this case $G_{i:j}$ indicates the reference Gibbs energy for a real or hypothetical compound $i:j$ with respect to the standard element enthalpy at 298.15 K (${}^{0}H_i^{SER}$ or ${}^{0}H_j^{SER}$, respectively).

The difference in the reference Gibbs energy for a given real or hypothetical compound $i:j$ (${}^{0}G_{i:j}$) of an intermetallic phase and the Gibbs energies of the elements i,j in their Standard Element Reference states (SER) (${}^{0}G_i$, ${}^{0}G_j$) is given by the equation:

$$ \Delta {}^{0}G_{i:j} = {}^{0}G_{i:j} - \nu_i \, {}^{0}G_i - \nu_j \, {}^{0}G_j = \Delta H - T\Delta S \quad (5) $$

where H is enthalpy and S is entropy.

At T = 0 K, one may write $\Delta H(T=0) = \Delta E(T=0)$, i.e. the difference in enthalpies is equal to the difference of total energies. These total energy differences have been calculated *ab initio* at the equilibrium volume in the present paper. The difference in enthalpies ΔH, at finite temperature is then obtained as (Kirchhoff's law):

$$ \Delta H = \Delta E + \int \Delta C_p \, dT \quad (6) $$

where ΔC_p is the difference between heat capacity of the given intermetallic phase and that of the SER structure.

In the region without phase transformation, entropy can be expressed as:

$$ \Delta S = \int (\Delta C_p / T) dT \quad (7) $$

In general, the heat capacity difference ΔC_p is temperature dependent, and in the simplest case it can be described by a linear function:

$$ \Delta C_p = a + bT \quad (8) $$

Substitution of the enthalpic and entropic term with the relations (6-8) in Eq. 5 yields after integration:

$$ \Delta {}^{0}G_{i:j} = \Delta E + a(1 - \ln T)T - (b/2)T^2 \quad (9) $$

This equation has been employed in the phase diagram calculations. ΔE is calculated *ab initio* and ΔC_p is optimized as a curve fitting parameter to the experimental phase equilibrium data.

3.Results

3.1. The binary boundary systems

Information on the three binary phase diagrams is based on the compilation by Massalski [21]. Assessments of experimental phase diagram data and thermodynamic modelling are available from various research groups: Ni-Sn [22,23], Ti-Sn [24], and Ti-Ni [25-27]. Detailed crystallographic data on unary and binary boundary phases reported in the literature (References 21-43) and obtained in the current work are summarized in Table S1 (ESI†); data for ternary compounds are listed in Table 1.

3.2. Phase equilibria in the ternary system Ti-Ni-Sn.

In order to determine the phase equilibria in the ternary system, about 60 alloys were investigated in as-cast state and after annealing at 800 and 950°C (7 days). In some cases these temperatures were not sufficient for equilibration of the samples and therefore they were additionally annealed for 7 days in the temperature range from 450 to 770°C (for Sn contents > 40 at %) and at 1050, 1080 and 1100°C (for alloys containing high melting compounds such as $TiNi_3$, TiNi, Ti_5Sn_3 and τ_2).

Combined evaluation of EDX and XPD data in equilibrated samples defined the number of three-phase fields, which are labelled alphabetically in the figures from *"a"* to *"w"*. The temperatures of the invariant four-phase reactions have been determined with DTA on equilibrated samples. Microstructures of the as-cast samples were used to define the primary crystallization fields and reactions during solidification. The phase equilibria established in the system are presented as projections of liquidus- and solidus surfaces (Figures 1 and 2), as a melting-crystallization diagram (Figure 3) and in form of a Schultz-Scheil diagram (Figure 4) for the solidification behavior in the entire system involving 20 isothermal four-phase reactions in the ternary. Phase equilibria at 950°C are presented as an isothermal section in Figure 5. A summary of the phases involved in invariant reactions is available from Table 2. Phase compositions of the selected alloys, which have been investigated in different states, are presented in Table S2 (ESI†) which contains links to the SEM images (Figures 6 to 8) that document respective statements.

Investigation of the alloys in as-cast state (Figures 6 and 8) shows, that the Heusler Phase (HP, τ_2-$TiNi_2Sn$, $MnCu_2Al$ type) has the largest field of primary crystallization. This phase melts congruently at 1447°C [5] and exhibits a wide homogeneity region at sub-solidus temperatures. Thus in the sample with nominal composition $TiNi_2Sn$, the HP crystallizes primarily ($Ti_{25.2}Ni_{49.7}Sn_{25.1}$, at.%), followed by small grains of τ_2 with composition $Ti_{15}Ni_{61}Sn_{24}$ (at.%) and the crystallization ends by solidification of Ni_3Sn_2 (Fig. 6a). After annealing at 950°C (Fig. 7a), an almost single-phase sample of τ_2 was obtained with small residual amounts of Ni_3Sn_2. In order to determine details in constitution, a sample with composition $Ti_{18}Ni_{58}Sn_{24}$ was prepared and investigated in three states. The as-cast specimen shows primary τ_2 with a composition close to stoichiometric $TiNi_2Sn$ ($Ti_{23.3}Ni_{52.2}Sn_{24.4}$), Ni_3Sn_2 and a eutectic structure with the composition $Ti_{7.5}Ni_{71.7}Sn_{20.8}$ (Fig. 6f). The samples annealed at 950°C and 1100°C (Figures 7f, 8f) reveal the three-phase field *"i"*: τ_2+Ni_2Sn_3+$TiNi_3$ ($Ti_{1-x}Sn_xNi_3$). However, the composition of τ_2 in the annealed specimens differs significantly: $Ti_{23.0}Ni_{52.3}Sn_{24.7}$ at 950°C but $Ti_{18.9}Ni_{57.0}Sn_{24.1}$ at 1100°C, respectively. The Rietveld refinement of the sample annealed at 1100°C confirms the crystal structure of the Heusler phase with Ti/Ni substitution in the 4b site (½,½,½). At high temperatures the homogeneity region of this phase extends further towards the binary phase TiNi. Thus, the sample $Ti_{37}Ni_{50}Sn_{13}$ in as-cast state defines τ_2 and TiNi with compositions $Ti_{29.5}Ni_{50.0}Sn_{20.6}$ and $Ti_{41.3}Ni_{50.7}Sn_{7.9}$, respectively. However, after annealing at 1100°C this sample exhibits almost single-phase τ_2 with a composition in the range from $Ti_{35.9}Ni_{50.3}Sn_{13.8}$ to $Ti_{38.2}Ni_{50.6}Sn_{11.2}$. A two-phase gap between TiNi and τ_2 is defined to exist in the composition range between 6 and 9 at% Sn considering EPMA data obtained from samples $Ti_{36}Ni_{58}Sn_6$ and $Ti_{43}Ni_{49}Sn_8$ annealed at 1100°C. Temperatures of invariant reaction that were measured on these samples by DTA were defined to be 1118°C (U_j) and 1146°C (U_k). Taking into account the extended homogeneity region of τ_2, a structural chemical formula for the Heusler phase may be expressed as $Ti_{1+y}Ni_{2-x}Sn_{1-y}$. The homogeneity region of this phase at 1100°C extends towards binary Ni-Sn, τ_1 and TiNi reaching compositions $Ti_{19}Ni_{57}Sn_{24}$, $Ti_{27}Ni_{46}Sn_{27}$ and $Ti_{41}Ni_{50}Sn_9$, respectively. Details on atom site preference in the crystal structure of τ_2 will be discussed in section 3.3.

In contrast to the full Heusler phase (τ_2), the Half Heusler phase (HH, τ_1, MgAgAs-type) has a much lower thermodynamic stability, resulting in a smaller primary crystallization field. τ_1 forms incongruently (Fig. 8k) by the invariant peritectic reaction l+τ_2 ↔ τ_1 at 1180°C. τ_1 shows a homogeneity region that tends toward τ_2. Thus, the sample $Ti_{29}Sn_{42}Ni_{29}$ after annealing at 1100°C (Fig 8n) reveals two compositions for the two Heusler phases (τ_1–$Ti_{30.8}Sn_{38.1}Ni_{31.1}$ and τ_2–$Ti_{26.8}Sn_{46.2}Ni_{26.9}$ in at. %) and Ni_3Sn_4, which forms from liquid during quenching. The crystallization of as-cast samples with tin contents outside the section Ni_3Sn_2 - τ_2 - τ_1 - Ti_5Sn_3 finishes with the formation of a tin rich liquid (Figures 6b, 6c, 6o, 8a, 8b, 8d, 8g, 8k). Consequently, all samples from this region, that were annealed at 800 and 950°C, were found to be in equilibrium with the Sn-rich liquid (see fields labelled *"s"*, *"t"*, *"u"* in Figure 5). Such a behavior suggests a cascade of transition type reactions (U) with temperatures decreasing from this section to the Sn-rich corner of the diagram. In order

to produce equilibrium samples for the determination of these reaction temperatures, the samples were annealed in the temperature range from 450 to 770°C. Comparing the microstructures of the as-cast alloys with those annealed at different temperatures (7a, 7b, 7c, 8c, 8e, and 8h) and considering the temperatures determined by DTA, four invariant reactions were established: U_b, U_c, U_d, U_e.

Besides of the Heusler phase (τ_2), the solid solution based on binary Ti_5Sn_3 ($Ti_5Ni_xSn_3$) also plays a dominant role in the formation of phase equilibria in the ternary system. Although this phase forms incongruently in the binary system and crystallizes in a narrow field from the liquid, the primary field of crystallization in the ternary extends up to 40 at % Ni (Figures 1 and 3). The solubility of nickel in Ti_5Sn_3 reaches a maximum extent at Ti_5NiSn_3, significantly increasing the thermodynamic stability of this phase (see DFT calculations in section *3.4.2.1*).

As-cast samples located within the composition triangle Ti_5NiSn_3 - Ti_2Ni_2Sn - TiNi and in the primary crystallization field of Ti_5NiSn_3 show similar but rather complicated microstructures. As an example Figure 8j represents the crystallization of four phases in the as cast sample $Ti_{48}Ni_{32}Sn_{18}$: primary $Ti_5Ni_xSn_3$ ($Ti_{55.5}Ni_{11.4}Sn_{33.0}$) followed by the crystallization of τ_2 ($Ti_{37.8}Ni_{49.5}Sn_{12.7}$), τ_3-Ti_2Ni_2Sn ($Ti_{43.8}Ni_{40.1}Sn_{16.1}$), TiNi ($Ti_{44.8}Ni_{49.2}Sn_{6.0}$) and a two-phase eutectic TiNi+$Ti_5Ni_xSn_3$ ($Ti_{49.1}Ni_{38.0}Sn_{12.9}$).

Table 1. Crystallographic data of the ternary phases of the system Ti-Ni-Sn.

Phase, Temperature range (°C)	Space group, Prototype	Lattice parameters (nm) a	c	Comments/References
τ_1-TiNiSn	$F\bar{4}3m$	0.5927	-	Ref.44
	MgAgAs	0. 59332(6)	-	Ref.4
		0.59349(1)	-	[*]
$Ti_{1+y}Ni_{2-x}Sn_{1-y}$		0.59655(4)	-	x=0.779, y=-0.008 at 1100°C; in equilibrium with τ_2 [*]
τ_2-$Ti_{1+y}Ni_{2-x}Sn_{1-y}$	$Fm\bar{3}m$	0.6097(3)	-	x=0, y=0, z=0 [4]
	$MnCu_2Al$	0.60973(4)	-	x=0, y=0, z=0 [*], see also Figure 9
		0.60710(5)	-	x=0.344, y=0.038 at 950°C; in equilibrium with τ_1 [*]
		0.60503(8)	-	x=0.008 , y=0.344 at 1100°C; in equilibrium with TiNi [*]
		0.6049(2)	-	x=-0.651, y=-0.121 at 1100°C; in equilibrium with $TiNi_3$ and Ni_3Sn_2 [*]
τ_3-$Ti_{2+x}Ni_2Sn_{1-x}$	$P4_2/mnm$	0.68168(4)	0.64379(6)	x=0 [4]
	U_2Pt_2Sn	0.68273(6)	0.63850(4)	x=0.195 in equilibrium with TiNi and Ti_5NiSn_3 at 950°C
τ_4- $(Ti_{1-x-y}Sn_xNi_y)Ni_3$	$Pm\bar{3}m$	0.36316(5)		$Ti_{14.0}Ni_{80.5}Sn_{5.5}$; x=0.22 and y=0.22; see also Figure 10
	$AuCu_3$	0.36904(7)		$Ti_{6.2}Ni_{77.4}Sn_{16.4}$; x=0.66 and y=0.1
$\tau_{4'}$	*unknown*			at ~ $Ti_{16\text{-}14}Ni_{75}Sn_{9\text{-}11}$
τ_5	*unknown*			at ~ $Ti_{52}Ni_{23}Sn_{25}$

[*] This work

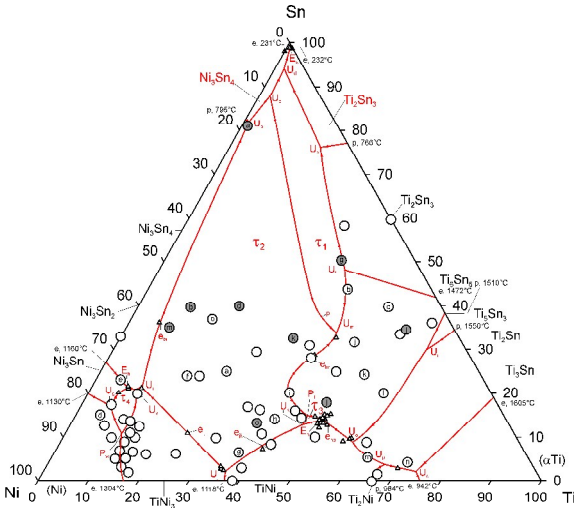

Figure 1. Liquidus projection of Ti-Ni-Sn. The labels inside the circles denote indices for the microstructures of as-cast samples presented in Figure 6 (open circles) and Figure 8 (gray circles). The small triangles show compositions of eutectics observed in as-cast samples. Composition of the phases measured by EPMA is listed in Table S2(ESI†).

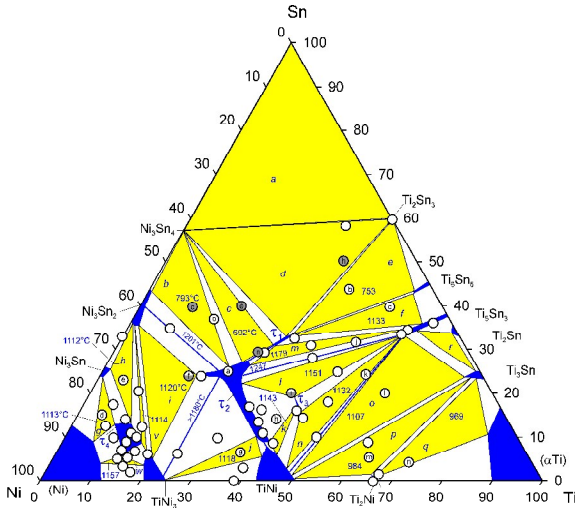

Figure 2. Solidus projection with corresponding temperatures, determined by DSC measurements. The labels inside the circles denote indexes for the microstructures of the samples annealed at 950°C (Fig. 7, open circles) and other temperatures Fig. 8 (gray and semi-filled circles).

Eutectics with similar compositions are observed in several other samples (see small triangles in Figure 3) and they are mainly located inside the three-phase region: τ_3+TiNi+Ti_5NiSn_3. For example Fig. 6k shows the microstructure of the as-cast sample $Ti_{53}Ni_{23}Sn_{24}$ with a primary crystallization of $Ti_5Ni_xSn_3$ ($Ti_{56.1}Ni_{10.7}Sn_{33.1}$) and a eutectic with the composition: $Ti_{48.8}Ni_{38.2}Sn_{13.0}$. As the composition of the liquid of the afore mentioned samples never crosses the tie-line TiNi - Ti_5NiSn_3 during crystallization, we can define the eutectic type reaction, E_n: L ↔ TiNi + Ti_2Ni_2Sn + $Ti_5Ni_xSn_3$, and the quasi-binary reaction, $e_{max,no}$: *l* ↔ TiNi+Ti_5NiSn_3. At higher titanium content~~s~~, we already observe the crystallization of Ti_3Sn. In the sample $Ti_{60}Ni_{20}Sn_{20}$, Ti_3Sn with the composition $Ti_{72.9}Ni_{2.4}Sn_{24.7}$ solidifies after Ti_5NiSn_3 ($Ti_{56.5}Ni_{11.0}Sn_{32.5}$) (Fig. 6ℓ). Besides Ti_3Sn, the microstructure shows two eutectics with very close compositions ~$Ti_{56}Ni_{35}Sn_9$ (TiNi+Ti_5NiSn_3, bright eutectic) and ~$Ti_{57}Ni_{33}Sn_{10}$ (TiNi+Ti_3Sn, dark eutectic). From the location of these eutectics (see Figure 3) the transition type reaction U_o was assigned: L+Ti_5NiSn_3 ↔ TiNi+Ti_3Sn. The crystallization of as-cast samples from this region (Figures 7ℓ, 7m and 7n), the phase composition and temperatures measured on the samples annealed at 950°C (Figures 6ℓ, 6m and 6n), allow us to define another cascade of transition type reactions: U_o (1107 °C), U_p (984 °C) and U_q (969 °C). Phase equilibria involving Ti_2Sn (phase region *"r"*) were not investigated, because the equilibration occurs at temperatures exceeding the technical limits of our furnaces and DTA.

The sample with stoichiometry τ_3-Ti_2Ni_2Sn, in as-cast state (Fig. 7i), shows primary crystallization of Ti_5NiSn_3 ($Ti_{55.4}Ni_{11.7}Sn_{32.9}$), than solidifies as τ_2 with two compositions ($Ti_{27.7}Ni_{48.1}Sn_{24.1}$ and $Ti_{32.5}Ni_{48.8}Sn_{18.8}$) and subsequently we observe the crystallization of τ_3 with composition $Ti_{43.6}Ni_{40.1}Sn_{16.2}$. The crystallization is finished by solidification of TiNi ($Ti_{43.1}Ni_{49.6}Sn_{7.7}$) and the formation of a two-phase eutectic TiNi+$Ti_5Ni_xSn_3$ with the composition $Ti_{49.3}Ni_{37.0}Sn_{13.8}$. Such a crystallization behavior indicates a peritectic formation of this phase via the reaction P_l: L+τ_2+$Ti_5Ni_xSn_3$ ↔ τ_3. The sample annealed at 800 and 950°C was not completely equilibrated and contains four phases (τ_2, τ_3, $Ti_5Ni_xSn_3$ and TiNi), however, after annealing at 1050°C (Fig. 8i), TiNi disappears and only three equilibrium phases remain: τ_2 ($Ti_{28.9}Ni_{48.8}Sn_{22.2}$), τ_3 ($Ti_{41.2}Ni_{40.0}Sn_{18.8}$) and $Ti_5Ni_xSn_3$ ($Ti_{55.7}Ni_{11.0}Sn_{33.3}$). The temperature of the invariant equilibrium P_1 at 1151°C is derived from DTA on the sample annealed at 1050°C. A similar morphology that confirms the peritectic crystallization of τ_3 is observed for the as-cast sample $Ti_{40}Ni_{46}Sn_{14}$ (Fig 7h) indicating a peritectic solidification of TiNi ($Ti_{41.6}Ni_{49.9}Sn_{8.5}$) around τ_2 with compositions varying from $Ti_{30.7}Ni_{49.5}Sn_{19.9}$ to $Ti_{29.4}Ni_{49.4}Sn_{21.2}$. The solidification in this sample also ends in the two-phase eutectic TiNi+$Ti_5Ni_xSn_3$ with composition $Ti_{50.6}Ni_{34.5}Sn_{14.9}$. All these observations establish a transition type reaction U_k: L+τ_2 ↔ τ_3+TiNi at 1143°C.

Another four-phase equilibrium, that involves the Heusler phase (τ_2) and binary TiNi is documented for the sample $Ti_{37}Ni_{57}Sn_6$. In as-cast state (Fig. 6g), we observe primary crystallization of τ_2 with compositions $Ti_{33}Ni_{51}Sn_{16}$ and $Ti_{36}Ni_{53}Sn_{11}$ for big and small grains, and a fine eutectic with overall composition $Ti_{36}Ni_{61}Sn_{13}$: the eutectic consists of TiNi ($Ti_{40}Ni_{55}Sn_5$) and $TiNi_3$, and significantly coagulates after annealing at 950°C for 10 days (Fig. 7g). As the composition of the eutectic lies outside of the three-phase triangle τ_2+$TiNi_3$+$(Ti_{1-x}Ni_x)_{1-y}Sn_y$ (field *"j"* on Figure 3), a transition type reaction U_j is defined: L+τ_2 ↔ $TiNi_3$+$(Ti_{1-x}Ni_x)_{1-y}Sn_y$. However, the temperature of this reaction, determined by DTA is 2°C lower than the respective reaction *l* ↔ $TiNi_3$+TiNi (1118°C) in the binary system.

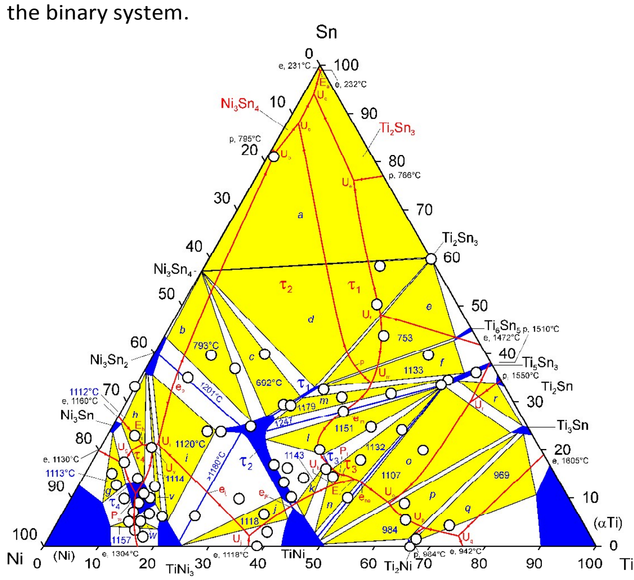

Figure 3. Sub-solidus surface with superimposed mono-variant lines from the liquidus. The composition of phases involved in the invariant reactions is summarized in Table 2

Binary $TiNi_3$ has the highest melting point (1380°C) within the Ti-Ni system and also exhibits rather extended Ti/Sn substitution $(Ti_{1-x}Sn_x)Ni_3$ up to x_{max}= 0.27 at 1080°C. However, at a higher tin content, the hexagonal structure of $(Ti_{1-x}Sn_x)Ni_3$ undergoes a structural transformation into a cubic structure with $AuCu_3$-type: τ_4-$(Ti_{1-x-y}Sn_xNi_y)Ni_3$. The homogeneity region of this phase extends at 1080°C from x=0.22 and y=0.22 (in equilibrium with $(Ti_{1-x}Sn_x)Ni_3$ and (Ni)) to x=0.54 and y=0.06 (in equilibrium with Ni_3Sn and (Ni)). However, the maximal solubility of tin in τ_4 at temperatures below solidus increases to 16.4 at % (x=0.66 and y=0.1) at 950°C) as determined from an annealed alloy $Ti_5Ni_{80}Sn_{15}$ (Fig. 7d) in equilibrium with Ni_3Sn and (Ni).

The sample in as cast state shows primary crystallization of (Ni) with grains of τ_4-$(Ti_{1-x-y}Sn_xNi_y)Ni_3$ solidifying around them, and both phases are embedded in a Ni_3Sn matrix (Fig 6d). In alloy $Ti_{10}Ni_{76}Sn_{14}$, τ_4 crystallizes as a primary phase with composition $Ti_{13.0}Ni_{77.2}Sn_{9.8}$ and solidification finishes in a two-phase eutectic (τ_4+Ni_3Sn) with composition $Ti_{5.8}Ni_{74.5}Sn_{19.8}$. This type of solidification indicates incongruent formation of this phase during a peritectic reaction. But our guess on the formation of this phase in a three-phase peritectic, L+$(Ti_{1-x}Sn_x)Ni_3$ ↔ τ_4, was ruled out by the observation that for the as-cast alloys with nickel contents from 75 to 81 at % Ni the last portion of the liquid becomes depleted by nickel. Such a solidification behavior agrees well with a cascade of reactions, peritectic P_w: L+(Ni)+$(Ti_{1-x}Sn_x)Ni_3$ ↔ τ_4 followed by a transition type reaction U_g: L+(Ni) ↔ $Ti_{1-x}Sn_x)Ni_3$+Ni_3Sn.

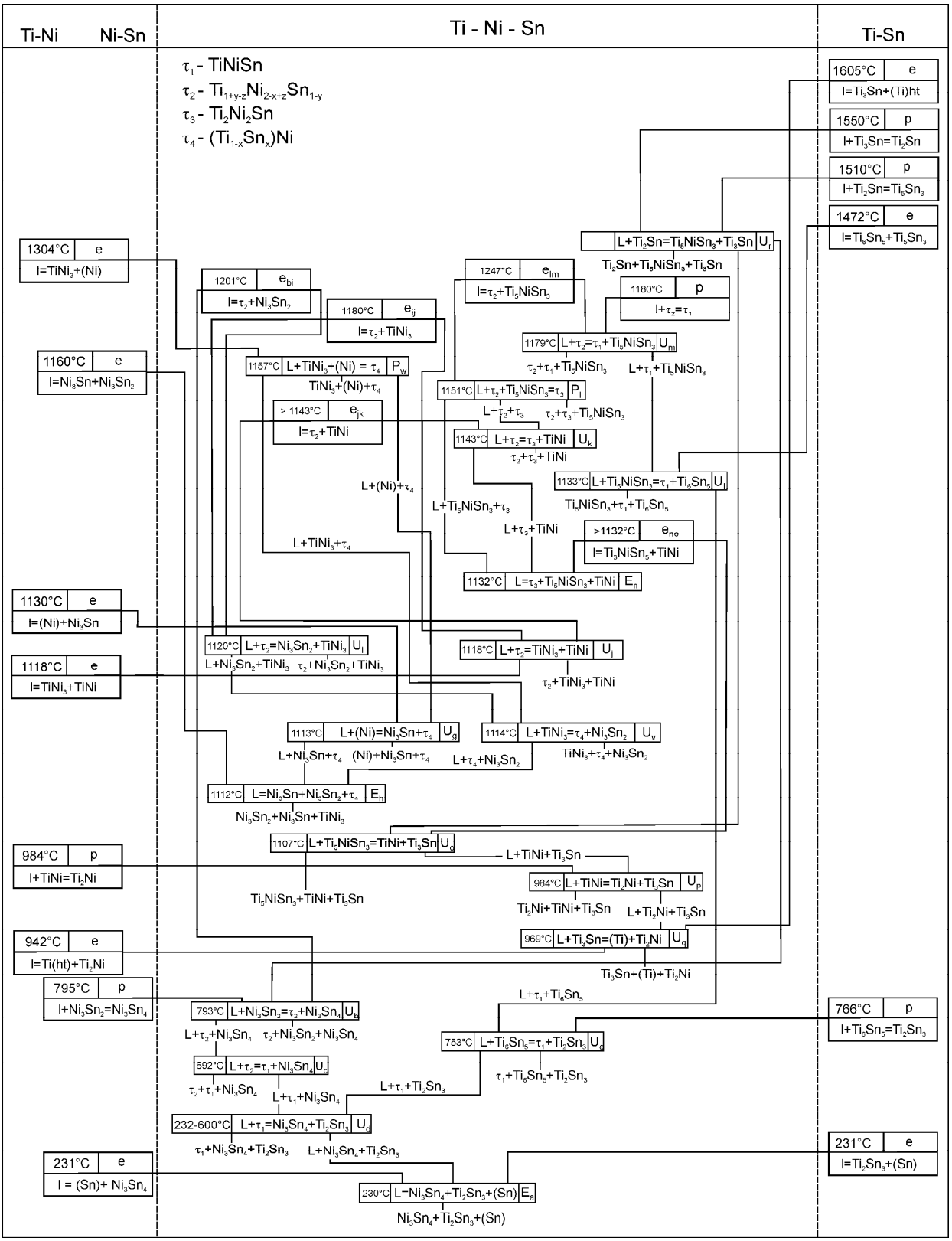

Figure 4. Schultz-Scheil diagram for the ternary Ti-Ni-Sn system. The homogeneity regions: $Ti_{1-x}Sn_xNi_3$, $Ti_5Ni_xSn_3$, $(Ti_{1-x}Ni_x)_{1-y}Sn_y$ and $Ti_{1+y}Ni_{2-x}Sn_{1-y}$ are noted as $TiNi_3$, Ti_5NiSn_3, $(Ti_{1-x}Ni_x)_{1-y}Sn_y$ and τ_2.

Table 2. Comparison of experimental and calculated data characterizing the invariant equilibria in the Ti-Ni-Sn system.

Reaction (exp.)	Phase	Ti	Ni	Sn	Type t °C	Reaction (calc.)	Phase	Ti	Ni	Sn	Type t °C
L + Ti_2Sn ↔	L	62	8	30	U_r	L + Ti_2Sn ↔	L	63.6	4.0	32.4	U
Ti_5Sn_3(Ni) + Ti_3Sn	Ti_2Sn	65.0	1.0	34.0	n.d.	Ti_5Sn_3(Ni) + Ti_3Sn	Ti_2Sn	67.2	0.3	32.5	1510.4
	Ti_5Sn_3(Ni)	57.5	8	34.5			Ti_5Sn_3(Ni)	60.5	3.2	36.3	
	Ti_3Sn	74	1	25			Ti_3Sn	75.1	0.0	24.9	
L + τ_2 ↔	L	42	24	34	U_m	L + τ_2 +	L	34.5	29.5	36.0	P
Ti_5Sn_3(Ni) + τ_1	τ_2	28.4	45.3	26.3	1179	Ti_5Sn_3(Ni)↔τ_1	τ_2	24.4	51.2	24.4	1168.5
	τ_1	31.2	37.4	31.5			τ_1	33.3	33.3	33.4	
	Ti_5Sn_3(Ni)	56.4	8.6	35.0			Ti_5Sn_3(Ni)	56.3	9.9	33.8	
L + Ti_5Sn_3(Ni)	L	37	15	48	U_f	L + Ti_5Sn_3(Ni)	L	34.0	26.1	39.9	U
↔ τ_1 + Ti_6Sn_5	Ti_5Sn_3(Ni)	57.9	5.9	36.2	1133	↔ τ_1 + Ti_6Sn_5	Ti_5Sn_3(Ni)	56.4	9.7	33.9	1154.8
	τ_1	33.2	33.6	33.2			τ_1	33.3	33.3	33.3	
	Ti_6Sn_5	52.7	4.5	42.8			Ti_6Sn_5	54.6	0.8	44.6	
L + τ_2 +	L	46	39	15	P_1	L + τ_2 ↔	L	40.9	39.3	19.8	U
Ti_5Sn_3(Ni) ↔ τ_3	τ_2	41.2	40	18.8	1151	Ti_5Sn_3(Ni) + τ_3	τ_2	24.9	51.7	23.4	1156.4
	Ti_5Sn_3(Ni)	55.6	11.1	33.3			Ti_5Sn_3(Ni)	56.1	10.2	33.7	
	τ_3	28.9	48.9	22.2			τ_3	40.0	40.0	20.0	
L + τ_2 ↔ τ_3 +	L	46	41	13	U_k	L + τ_2 ↔ τ_3 +	L	40.7	42.0	17.3	U
(TiNi)	τ_2	41.1	49.8	9.1	1143	(TiNi)	τ_2	25.0	51.9	23.1	1151.0
	τ_3	42.3	40.4	17.3			τ_3	40.0	40.0	20.0	
	(TiNi)	44.0	50.0	6.0			(TiNi)	31.3	48.7	20.0	
L + τ_2 ↔	L	36	62	2	U_j	L ↔ ($TiNi_3$) +	L	31.7	60.9	7.4	E
($TiNi_3$) +(TiNi)	τ_2	37.8	52	10.2	1118	τ_2 + (TiNi)	τ_2	25.1	52.5	22.4	1130.8
	($TiNi_3$)	25	74.9	0.1			($TiNi_3$)	25.0	75.0	0.0	
	(TiNi)	41.3	53.2	5.5			(TiNi)	37.0	54.5	8.5	
L ↔ τ_3 +	L	49	37	14	E_n	L ↔ τ_3 +	L	43.5	39.8	16.7	E
(TiNi) +	τ_3	43.9	40.2	15.9	1132	(TiNi) +	τ_3	40.0	40.0	20.0	1139.9
Ti_5Sn_3(Ni)	(TiNi)	47.5	49.8	2.7		Ti_5Sn_3(Ni)	(TiNi)	32.6	49.3	18.1	
	Ti_5Sn_3(Ni)	55.6	11.1	33.3			Ti_5Sn_3(Ni)	56.1	10.2	33.7	
L + Ti_5Sn_3(Ni)	L	58	33	9	U_o	L↔Ti_5Sn_3(Ni)+	L	53.2	35.1	11.7	E
↔ (TiNi) + Ti_3Sn	Ti_5Sn_3(Ni)	55.6	11.1	33.4	1107	(TiNi) + Ti_3Sn	Ti_5Sn_3(Ni)	56.5	9.6	33.9	1108.1
	(TiNi)	49.3	49.6	1.1			(TiNi)	38.2	51.8	10.0	
	Ti_3Sn	72.5	3.8	23.7			Ti_3Sn	75.0	0.1	24.9	
L+($TiNi_3$)+	L	12.0	77.0	11.0	P_w	L+($TiNi_3$) ↔	L	11.8	74.6	13.6	U
(Ni)↔τ_4	($TiNi_3$)	18.7	77.9	3.4	1157	(Ni) + τ_4	($TiNi_3$)	13.5	77.6	8.9	1061.8
	(Ni)	10.2	86.2	3.6			(Ni)	10.6	79.3	10.1	
	τ_4	13.7	80.8	5.5			τ_4	13.4	72.4	14.2	
L + (Ni) ↔	L	6.1	77.0	16.9	U_g	L + (Ti Ni_3) ↔	L	8.0	74.2	17.8	E
Ni_3Sn + τ_4	(Ni)	6.2	84.9	8.9	1113	(Ni) + Ni_3Sn	(Ni)	7.5	78.9	13.6	1045.8
	Ni_3Sn	0.8	75.6	23.6			Ni_3Sn	1.5	73.7	24.8	
	τ_4	8.6	78.5	12.9			τ_4	11.3	72.3	16.4	
L+ ($TiNi_3$) ↔	L	9.0	70.0	21.0	U_v	L + ($TiNi_3$) ↔	L	14.8	71.1	14.1	U
Ni_3Sn_2 + τ_4	($TiNi_3$)	17.9	75.4	6.7	1114	τ_2 + τ_4	$TiNi_3$	18.6	76.2	5.2	1066.7
	Ni_3Sn_2	0.9	63.1	36.0			τ_2	24.0	52.4	23.6	
	τ_4	15.9	75.7	8.4			τ_4	14.5	72.1	13.4	
L ↔Ni_3Sn +	L	7.0	72.0	21.0	E_h	L ↔ Ni_3Sn +	L	8.5	70.7	20.8	E
τ_4+ Ni_3Sn_2	Ni_3Sn	1.2	73.3	25.5	1112	τ_4+ Ni_3Sn_2	Ni_3Sn	1.9	72.7	25.4	1045.5
	τ_4	11.8	75.5	12.7			τ_4	11.2	72.0	16.8	
	Ni_3Sn_2	0.4	63.4	36.2			Ni_3Sn_2	2.9	62.6	34.5	
L + τ_2 ↔(Ti	L	10.0	69.0	21.0	U_i	L ↔ τ_2 + τ_4 +	L	10.6	67.5	21.9	E
Ni_3) + Ni_3Sn_2	τ_2	18.9	57	24.1	1120	Ni_3Sn_2+	τ_2	23.5	52.1	24.4	1044.6
	($TiNi_3$)	19.6	75.3	5.1			τ_4	12.0	71.7	16.3	
	Ni_3Sn_2	1.8	62.6	35.6			Ni_3Sn_2	4.1	62.3	33.6	
L + (Ti Ni) ↔	L	67.0	29.5	3.5	U_p	L ↔ (Ti Ni) +	L	66.8	30.9	2.3	E
Ti_3Sn + Ti_2Ni	(TiNi)	50.3	49.2	0.5	984	Ti_3Sn + Ti_2Ni	(TiNi)	45.3	54.4	0.3	957.5
	Ti_3Sn	73.9	2.5	23.6			Ti_3Sn	75.9	1.1	23.0	
	Ti_2Ni	65.1	33.4	1.5			Ti_2Ni	66.7	33.3	0.0	
L + Ti_3Sn ↔	L	74	24	2	U_q	L ↔ Ti_3Sn +	L	68.6	29.3	2.1	E
Ti_2Ni + (Ti)	Ti_3Sn	74.9	1.5	23.6	969	Ti_2Ni + (Ti)	Ti_3Sn	76.2	1.2	22.6	957.2
	Ti_2Ni	66	33.1	0.9			Ti_2Ni	66.7	33.3	0.0	
	(Ti)	83.6	5.8	10.6			(Ti)	76.1	0.7	23.2	

Reaction (exp.)	Phase	Ti	Ni	Sn	Type t °C	Reaction (calc.)	Phase	Ti	Ni	Sn	Type t °C
$L + Ni_3Sn_2 \leftrightarrow$	L	1	17	82	U_b	$L + Ni_3Sn_2 \leftrightarrow$	L	8.3	27.4	64.3	U
$\tau_2 + Ni_3Sn_4$	Ni_3Sn_2	0	56.2	43.8	793	$\tau_2 + Ni_3Sn_4$	Ni_3Sn_2	0.1	56.2	43.7	748.0
	τ_2	24.6	49.6	25.8			τ_2	23.6	51.0	25.4	
	Ni_3Sn_4	0.5	42.4	57.1			Ni_3Sn_4	0.0	44.0	56.0	
$L + Ti_6Sn_5 \leftrightarrow$	L	18	6	76	U_e	$L + Ti_6Sn_5 \leftrightarrow$	L	14.7	3.5	81.8	U
$\tau_1 + Ti_2Sn_3$	Ti_6Sn_5	52.8	4	43.2	753	$\tau_1 + Ti_2Sn_3$	Ti_6Sn_5	54.5	0.0	45.5	738.7
	τ_1	33.4	33.2	33.4			τ_1	33.3	33.3	33.4	
	Ti_2Sn_3	40.3	0	59.7			Ti_2Sn_3	40.0	0.0	60.0	
$L+\tau_2 \leftrightarrow$	L	2	10	88	U_c	$L+\tau_2 \leftrightarrow$	L	8.4	24.8	66.8	U
$\tau_1+Ni_3Sn_4$	τ_2	26.8	46.3	26.9	692	$\tau_1+Ni_3Sn_4$	τ_2	23.6	51.0	25.4	716.7
	τ_1	30.8	38.1	31.1			τ_1	33.3	33.3	33.4	
	Ni_3Sn_4	0	42.9	57.1			Ni_3Sn_4	0.0	43.8	56.2	
$L \leftrightarrow Ni_3Sn_4+$	L	0.2	0.6	99.2	E_a						
$Ti_2Sn_3+(Sn)$	Ni_3Sn_4	0	42.9	57.1	~232						
	Ti_2Sn_3	40	0	60							
	(Sn)	0.8	0.8	98.4							
$L+\tau_1 \leftrightarrow$	L	2	4	94	U_d						
$Ni_3Sn_4+Ti_2Sn_3$	τ_1	32.6	34.6	32.8	232-						
	Ni_3Sn_4	0	42.9	57.1	600						
	Ti_2Sn_3	40	0	60							
$\ell + \tau_2 \leftrightarrow \tau_1$	ℓ	37.5	25.0	37.5	p_{cm}						
	τ_2	27.5	45.0	27.5	>1179						
	τ_1	31.0	38.0	31.0							
						$\ell + \tau_2 \leftrightarrow \tau_3$	ℓ	40.8	39.3	19.8	p
							τ_2				1156.4
							τ_3				
$\ell \leftrightarrow \tau_2 + Ni_3Sn_2$	ℓ	6.3	57.6	36.1	e_{bi}	$\ell \leftrightarrow \tau_2 + Ni_3Sn_2$	ℓ	9.7	56.8	33.5	e
	τ_2	23	52	25	1201		τ_2				1129.4
	Ni_3Sn_2	1	59.4	39.6			Ni_3Sn_2				
$\ell \leftrightarrow \tau_2 + (TiNi_3)$	ℓ	24.2	64.9	10.9	e_{ij}	$\ell \leftrightarrow \tau_2 + (TiNi_3)$	ℓ	24.8	66.0	9.2	e
	τ_2	23.6	52.7	23.7	>1180		τ_2				1197.2
	$TiNi_3$	23.8	75.4	0.8			$TiNi_3$				
$\ell \leftrightarrow \tau_2 + (TiNi)$	ℓ	40.5	51	8.5	e_{jk}	$\ell \leftrightarrow \tau_2 + (TiNi)$	ℓ	35.9	51.3	12.7	e
	τ_2	40	51	9	>1143		τ_2				1220.8
	(TiNi)	41	51	8			(TiNi)				
$\ell \leftrightarrow \tau_2 + Ti_5Sn_3(Ni)$	ℓ	40	32	28	e_{lm}	$\ell \leftrightarrow \tau_2 + Ti_5Sn_3(Ni)$	ℓ	37.8	34.3	27.8	e
	τ_2	28	48	24	1247		τ_2				1209.5
	$Ti_5Sn_3(Ni)$	55.6	11.1	33.3			$Ti_5Sn_3(Ni)$				
						$\ell \leftrightarrow$(TiNi)+Ti_3Sn	ℓ	54.8	35.0	10.3	e
							(TiNi)				1111.5
							Ti_3Sn				
$\ell \leftrightarrow$ (TiNi) +	ℓ	51	36	13	e_{no}	$\ell \leftrightarrow$ (TiNi) +	ℓ	45.9	38.8	15.3	e
$Ti_5Sn_3(Ni)$	(TiNi)	48.6	49.6	1.8	>1132	$Ti_5Sn_3(Ni)$	(TiNi)				1144.6
	$Ti_5Sn_3(Ni)$	55.6	11.1	33.3			$Ti_5Sn_3(Ni)$				
						$\ell \leftrightarrow Ti_2Ni+Ti_3Sn$	ℓ	67.7	30.1	2.2	e
							Ti_2Ni				957.8
							Ti_3Sn				

The temperature of the invariant reaction U_g (1113°C) is only one degree higher than that determined for E_h: $L \leftrightarrow Ni_3Sn+Ni_3Sn_2+\tau_4$ (1112°C), which is evident from the microstructure of the as-cast alloy with nominal composition $Ti_7Ni_{70}Sn_{23}$ (Fig. 6e): we observe primary crystallization of Ni_3Sn_2, continued by a solidification of $NiSn_3$ and the final liquid crystallizes in form of a eutectic with composition $Ti_{7.5}Ni_{71.7}Sn_{20.8}$. The composition of this eutectic lies outside of the tie-triangle $Ni_3Sn+Ni_3Sn_2+\tau_4$ determined on a sample annealed at 950°C (Fig. 7e, Table S2 (ESI†)), but it is located inside of this three-phase field as it was established for the sample annealed at 1080°C. It should be noted, that this invariant eutectic is much finer than the two-phase mono-variant eutectic $l \rightarrow (Ti_{1-x}Sn_x)Ni_3 + Ni_3Sn_2$ that is observed in the as-cast sample $Ti_{18}Ni_{58}Sn_{24}$ (Fig. 7f). The microstructure of the latter sample also documents a secondary crystallization of Ni_3Sn_2 after primary τ_2. Considering this and the fact that the composition of this mono-variant eutectic ($Ti_{10}Ni_{69}Sn_{21}$) is located slightly outside of the three-phase field ($Ti_{1-x}Sn_x)Ni_3+Ni_3Sn_2+\tau_2$ (*"i"* in Figure 3), the invariant reaction U_i: $L+\tau_2 \leftrightarrow (Ti_{1-x}Sn_x)Ni_3+Ni_3Sn_2$ was established. Another transition-type invariant three-phase reaction U_v: $L + (Ti_{1-}$

$_xSn_x)Ni_3 \leftrightarrow \tau_4 + Ni_3Sn_2$ located between the afore mentioned reactions was established at 1114°C. The respective three-phase field on the solidus is rather narrow and we were unable to detect the eutectic structure that would document this invariant reaction.

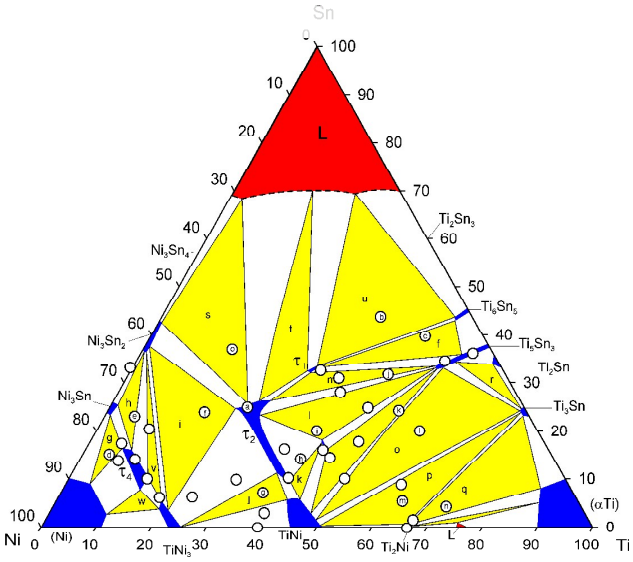

Figure 5. Isothermal section at 950°C. The labels inside the circles denote indices for the microstructures of the annealed samples presented in Fig. 7.

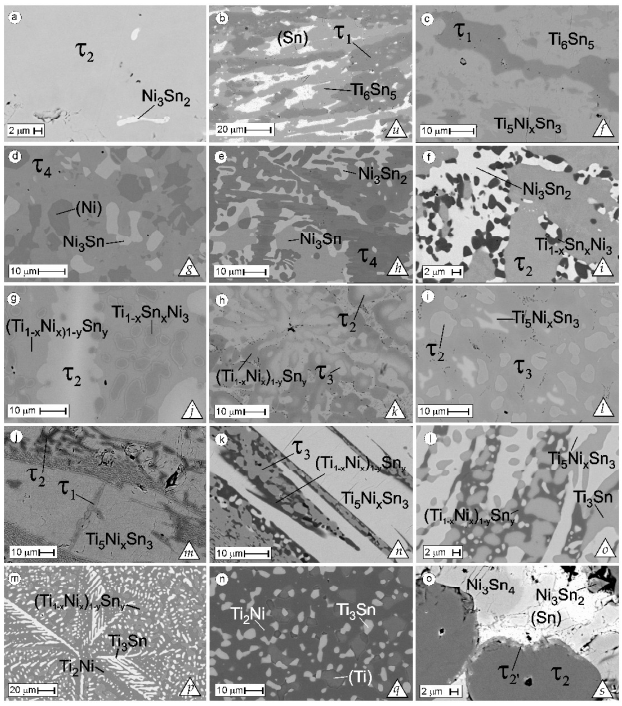

Figure 7. Microstructures of the selected samples annealed at 950°C. Labels inside of the triangles denote the respective three phase fields (Figures 1-5). Compositions of the phases are listed in Table S2 (ESI†). The compositions of the samples are marked with respective indices inside of the open circles on Figure 5.

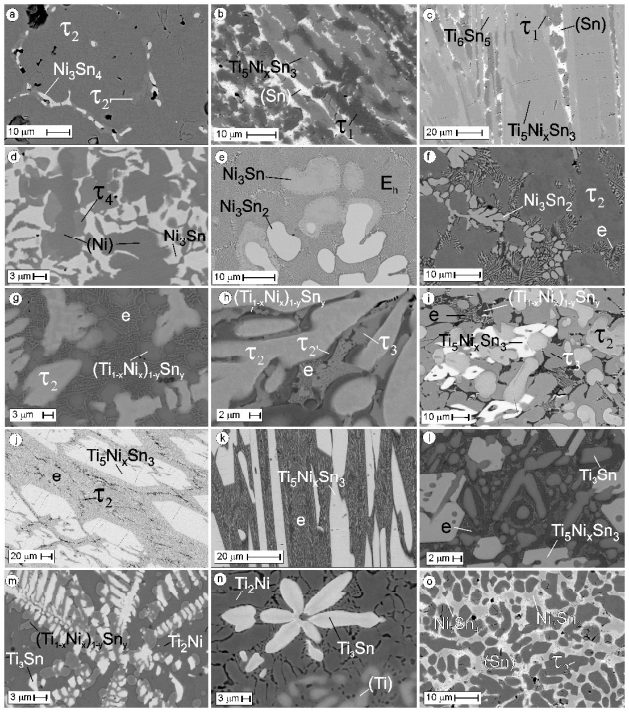

Figure 6. Microstructure of selected as-cast samples. The composition of the samples is marked with respective indices inside of the open circles on Figure 1.

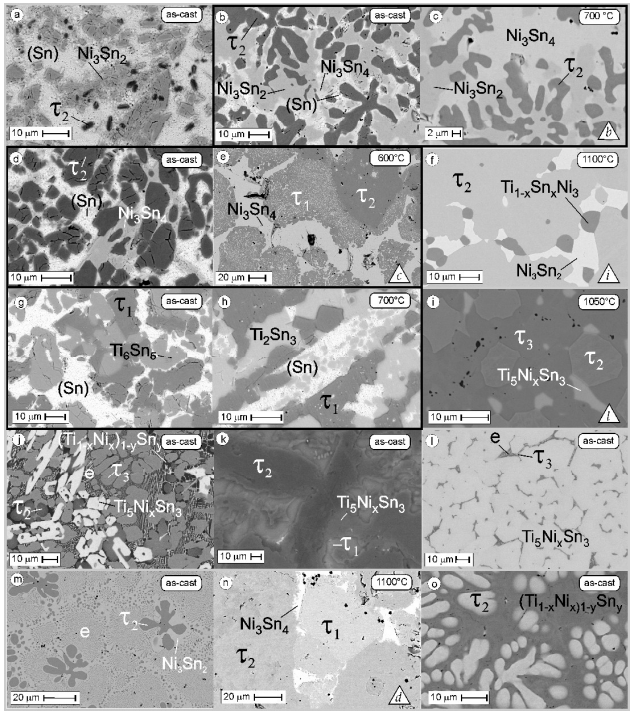

Figure 8. Microstructures of selected as-cast and annealed samples. Labels inside of the triangles denote the respective three-phase fields (Figures 1-5). Composition of the phases after EPMA is listed in Table S2 (ESI†). The composition of the as-cast samples is marked with respective indices inside of the gray circles on Figure 1. The annealed samples are denoted with indices inside gray and semi-filled circles on Figure 2.

An additional uncertainty in the determination of phase equilibria in this region arises from the characterization of the samples by XPD that show the existence of a further novel phase with composition $Ti_{1-x}Sn_xNi_3$ ($0.36 \leq x \leq 0.48$), which exists in the Ni-poor part of the solid solution of τ_4-$(Ti_{1-x}Sn_xNi_y)Ni_3$. In order to determine details on the crystal structure and phase equilibria involving this phase, (labelled as τ_4'-$Ti_{1-x}Sn_xNi_3$) additional investigations need to be performed.

The invariant four-phase reactions established in the system are summarized in a Schulz-Scheil diagram (Figure 4), and in order to complete this crystallization scheme, some additional invariant three-phase reactions (e_{max}) are requested. Besides the above discussed quasi-binary eutectic $e_{max,no}$: $l \leftrightarrow$ TiNi + Ti_5NiSn_3, the high melting τ_2 phase forms a set of invariant eutectics with the solid solutions of binary compounds Ti_5Sn_3 (e_{lm}), TiNi (e_{jk}), $TiNi_3$(e_{jk}) and Ni_3Sn_2 (e_{bi}). The microstructure of the as-cast alloy $Ti_8Ni_{57}Sn_{35}$ (Fig. 8m) represents a fine eutectic structure (with composition $Ti_{6.3}Ni_{57.1}Sn_{36.1}$) that forms via the invariant reaction e_{bi}: $l \leftrightarrow \tau_2 + Ni_3Sn_2$. The temperature of this reaction is 1201°C, being above the neighboring invariant reactions U_b (793°C) and U_i (1120°C). This provides an additional proof for this quasi-binary eutectic. The isothermal section at 950°C (see Fig. 6) represents phase equilibria similar to those reported earlier at 800°C [4] for exception that two additional three-phase fields involving τ_4 are present in the up-dated section. The difference in extension of the homogeneity regions for solid solutions may be interpreted as the typical shrinkage of single phase fields with decrease of temperature as well as by the general difficulties of equilibration of samples at low temperatures. In this context we need to mention difficulties in the homogenization of alloys containing the high melting compounds τ_2, $Ti_5Ni_xSn_3$, TiNi and $(Ti_{1-x}Sn_x)Ni_3$ at 950 °C and even at sub-solidus temperatures (1050-1100°C). Therefore thermodynamic modelling of the phase diagram is more suitable to describe the equilibrium compositions at temperatures below 1000°C.

3.3. Crystal structures and homogeneity regions of ternary phases.

With respect to the importance of crystallographic data for defining models for the thermodynamic parameters we performed a number of Rietveld refinements for τ_1-TiNiSn, τ_2-$Ti_{1+y}Ni_{2-x}Sn_{1-y}$, $(Ti_{1-x}Sn_x)Ni_3$ and $Ti_5Ni_xSn_3$ (see Table S3 (ESI†)). The half Heusler phase (τ_1) shows a narrow homogeneity region that is slightly off-stoichiometric on the tin-rich side $Ti_{32.5}Ni_{34.5}Sn_{32.9}$ at 1100°C, and $Ti_{32.6}Ni_{34.3}Sn_{33.1}$ at 950°C) and extends up to $Ti_{30.9}Ni_{37.8}Sn_{31.3}$ in equilibrium with τ_2 at 1100°C. Rietveld refinement for TiNiSn confirms full atom order in the structure (Table S3 (ESI†)). The Heusler phase (τ_2-$Ti_{1+y}Ni_{2-x}Sn_{1-y}$) exhibits the biggest homogeneity region that extends at 1100°C to $Ti_{27}Ni_{46}Sn_{27}$ (x=0.30 and y=0.00 in equilibrium with τ_1), to $Ti_{41}Ni_{50}Sn_9$ (x=0 and y=0.64 in equilibrium with TiNi) and to $Ti_{19}Ni_{57}Sn_{24}$ (x=-0.65 and y=-0.12 in equilibrium with $TiNi_3$ and Ni_3Sn_2).

Rietveld refinements (Table S3 (ESI†)) confirm a full order for stoichiometric $TiNi_2Sn$, whereas Ti/Sn substitution occurs in sites 4a (0,0,0) and 4b (½,½,½), respectively for tin-poor and nickel-rich extensions of the homogeneity region. The refinement did not reveal any substantial deviation from a full occupancy of Ni in site 8c (¼,¼,¼). It seems that this site is only affected for compositions that extend from stoichiometric τ_2-$TiNi_2Sn$ towards τ_1-TiNiSn. Considering the close crystallographic relation between both Heusler phases and TiNi (all are derivatives of the W-type structure, we plotted the compositional dependence of the lattice parameters for the section TiNi-$TiNi_2Sn$ (Fig. 9). One can see that lattice parameters increase with increasing tin content in the 4a site (0,0,0) and the dependence shows a positive deviation from Vegard's law. Maximal lattice parameters ($a \approx 0.610$ nm) are observed for compositions near stoichiometric τ_2-$TiNi_2Sn$ and the unit cell shrinks when Sn-atoms substitute for Ti in the 4b site (½,½,½). Due to the small difference in lattice parameters for τ_2 and the TiNi-based solution $(Ti_{1-x}Ni_x)_{1-y}Sn_y$ the XPD reflexes for these phases strongly overlap and we were unable to perform an unambiguous deconvolution of the diffraction maxima and to determine precise lattice parameters for the equilibrium compositions. However, these compounds appear as well separated individual phases on SEM images in as-cast (Figs 6h and 8o) and annealed (Fig. 7g) alloys, allowing a reliable determination of the compositions by EPMA. A much more significant decrease of the lattice parameters from $a \approx 0.610$ nm to $a \approx 0.593$ nm is observed for the structural change from τ_2-$TiNi_2Sn$ to τ_1-TiNiSn and because of this fact these two phases are well distinguishable in XPD profiles.

Compositional dependence of lattice parameters for the new compound τ_4-$(Ti_{1-x-y}Sn_xNi_y)Ni_3$ with $AuCu_3$-type structure is shown in Figure 10. Lattice parameters increase with increase of tin content and this dependence extrapolates to the value of a=0.3738 nm reported for the high pressure modification of Ni_3Sn which also adopts the $AuCu_3$ type structure.

The close structural relation between $AuCu_3$ and the crystal structure of Ni (Cu-type) allows a second order transformation between these structures. However, the phase separation between these structures was clearly documented by SEM images for sample $Ti_5Ni_{80}Sn_{15}$ annealed at 950°C (Fig. 7d) and was confirmed by XPD showing two sets of diffraction spectra of cubic structures with primitive (τ_4) and face-centered (Ni) lattices. We note that primitive X-ray diffraction peaks from the τ_4 lattice almost vanish at low Sn contents (zero intensity for $Ti_{0.786}Sn_{0.214}Ni_3$) due to the fact that the electron density in both crystallographic sites becomes similar. This may lead to possible misinterpretation of XPD patterns of this phase with the fcc nickel-based solid solution.

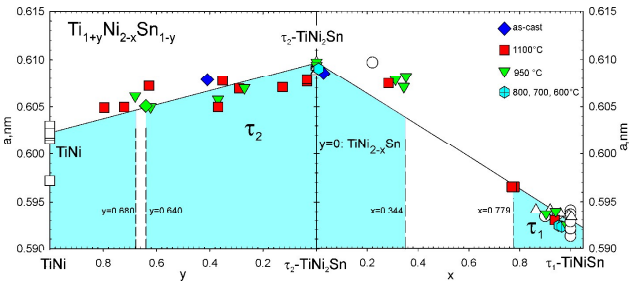

Figure 9. Compositional dependence of lattice parameters for homogeneity regions for the phases: TiNi, τ_1-TiNiSn and τ_2-$TiNi_2Sn$. The composition of the solid solution is expressed as $Ti_{1+y}Ni_{2-x}Sn_{1-y}$. Extensions of the homogeneity regions at 1100°C are marked with dashed lines. Literature (open symbols), squares [32, 36,44-51]; circles [1,5,9,52-56]; triangles-up. [57]

Furthermore, we subjected the ternary solid solution $Ti_5Ni_xSn_3$ (Hf_5CuSn_3-type structure; i.e. a filled variant of binary Ti_5Sn_3 with the Mn_5Si_3-type) to a detailed crystallographic investigation. Due to non-equilibrium solidification of as-cast samples $Ti_5Ni_xSn_3$ with x=0.9 and 1.0, EPMA line scans showed that the nickel content in this phase increases from 6.3 at% Ni at the grain centre to 10.2 at % Ni at the rim of the grains.

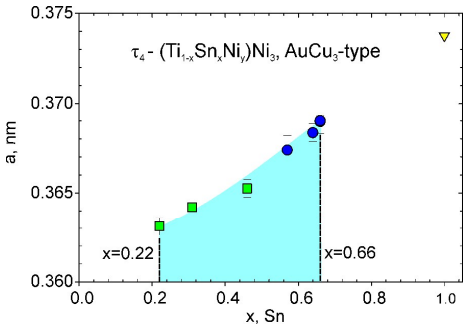

Figure 10. Compositional dependence of lattice parameters for the homogeneity region of τ_4-$(Ti_{1-x-y}Sn_xNi_y)Ni_3$ ($0.02 \le x \le 0.22$) for samples annealed at 950°C (circles) and 1080°C (squares). Triangles: isotypic high-pressure modification of Ni_3Sn. [28]

Table 3. X-Ray single crystal data for $Ti_5Ni_{0.96}Sn_3$ (Hf_5CuSn_3-type); space group $P6_3/mcm$ No. 193 (redundancy <10, $7.73 \le 2\theta \le 72.27°$, crystal size 30×35×35 μm). Standardized with program Structure Tidy. [58]

Parameter	$Ti_5Ni_{0.96}Sn_3$
EPMA, at%	$Ti_{56.0}Ni_{10.0}Sn_{34.0}$
Refinement; at%	$Ti_{55.8}Ni_{10.7}Sn_{33.5}$
a; c [nm]	0.81440(1);0.555922(9)
Reflections in refinement	304 $F_o > 4sig(F_o)$ of 309
Number of variables	16
$R_F = \Sigma\|F_0-F_c\|/\Sigma F_0$	0.0298
R_{int}	0.0303
wR2	0.0595
GOF	1.143
Extinction (Zachariasen)	0.0021
Ti1 in 6g (x,0, ¼), x; occ.	0.2550(4); 1.00(1)
U_{11}; U_{22}	0.052(1); 0.0227(9)
U_{33}; $U_{23}=U_{13}=0$; U_{12} [nm^2]	0.0252(8); 0.0114(4)
Sn1 in 6g (x,0, ¼), x; occ.	0.61161(8); 1.002(7)
U_{11}; U_{22}	0.0253(3); 0.0077(2)
U_{33}; $U_{23}=U_{13}=0$; U_{12} [nm^2]	0.0117(2); 0.0038(1)
Ti2 in 4d (1/3, 2/3, 0), occ.	0.996(8)
$U_{11}=U_{22}$; U_{33}	0.0098(1); 0.0063(5)
$U_{23}=U_{13}=0$; U_{12} [nm^2]	0.0045(2)
Ni in 2b (0,0, 0), occ.	0.96(2)
$U_{11}=U_{22}$; U_{33}	0.094(3); 0.066(3)
U23=U13=0; U12 [nm^2]	0.047(2)
Residual density: max; min	2.31;-3.42
Principal mean square atomic displacements (U)	Ti1 0.0620 0.0252 0.0227 Sn1 0.0312 0.0117 0.0077 Ti2 0.0091 0.0091 0.0063 Ni 0.0945 0.0945 0.0660

This heterogeneity results in some broadening of the XPD reflections. Annealing at 1100°C for 6 days provides a complete homogenization of the composition, but a comparison of XPD profiles for as-cast and annealed samples shows that the half-width of only some reflections is reduced whilst others show a clear split suggesting a structural transformation in this phase. Several single crystals were selected from the annealed sample but inspection on an AXS-GADDS texture goniometer did not reveal any significant distortion of the unit cell. One crystal specimen was characterized by means of four-circle Nonius Kappa diffractometer intensity data. Although the measured data were processed in triclinic symmetry, single crystal refinement fully complies with the symmetry and atom site distribution of the Hf_5CuSn_3-type structure (ordered Ti_5Ga_4-type; for crystallographic details see Table 3).

3.4. Thermodynamic assessment of the Ti-Ni-Sn system

3.4.1. Thermodynamic data for binary boundary systems. Thermodynamic data were taken from the most recent CALPHAD modelling of the binary systems by various research groups: Ni-Sn [23], Ti-Sn [24], and Ti-Ni [26].

3.4.2. Thermodynamic evaluation of the Ti-Ni-Sn system.

3.4.2.1 DFT Calculations of ternary compounds TiNiSn, $TiNi_2Sn$, Ti_2Ni_2Sn and of the solid solutions $Ti_5Ni_{1-x}Sn_3$, $Ti_{1-x}Sn_xNi_3$ and $(Ti_{1-x}Ni_x)_{1-y}Sn_y$.

$Ti_5Ni_{1-x}Sn_3$: The modelling of the $Ti_5Ni_{1-x}Sn_3$ solid solution consisted of two steps. At the first step the ground state energy of Ti_5Sn_3 with optimised crystal structure was calculated (Table 4). The negative enthalpy of formation (Table 5) proves the possibility of its formation. At the second step the chemical composition of the compound was modified by introducing additional Ni atoms into the 2*b* site to fit the Ti_5NiSn_3 composition. After that the ground state energy of Ti_5NiSn_3 with optimised crystal structure (Table 4) was calculated. Comparing the enthalpy of formation of Ti_5Sn_3 and Ti_5NiSn_3 (Table 5) one can see that it is lower for Ti_5NiSn_3, which means that the filling of the 2*b* site with Ni atoms is energetically favourable and predicts the formation of the interstitial solid solution $Ti_5Ni_{1-x}Sn_3$. For further thermodynamic calculations the ground state energy and the enthalpy of formation were calculated for the hypothetical compound Ni_5NiNi_3 (Table 5) with the same structure as Ti_5NiSn_3 and optimised crystal structure geometry (Table 4).

$Ti_{1-x}Sn_xNi_3$: The substitutional (Ti by Sn) solid solution based on $TiNi_3$ was modelled in two ways. In the first case the Ti2 atoms in the 2*d* position and in the second case the Ti1 atoms in the 2*a* site were substituted by Sn atoms yielding the compositions $Ti_{0.5}Sn_{0.5}Ni_3$ and $Sn_{0.5}Ti_{0.5}Ni_3$, respectively. The ground state energy and the enthalpy of formation (Table 5) were calculated for $SnNi_3$, $TiNi_3$, $Ti_{0.5}Sn_{0.5}Ni_3$, and $Sn_{0.5}Ti_{0.5}Ni_3$ with a completely relaxed geometry (Table 4). The comparison of $Ti_{0.5}Sn_{0.5}Ni_3$ and $Sn_{0.5}Ti_{0.5}Ni_3$ at the same composition (x = 0.5) shows that the configuration of $Ti_{0.5}Sn_{0.5}Ni_3$ is more preferable due to the lower enthalpy of formation value. The analysis of the ΔH values of $TiNi_3$, $SnNi_3$, and $Ti_{0.5}Sn_{0.5}Ni_3$ predicts that the formation of the solid solution at T = 0 K is not possible. However, at higher temperature the formation of $Ti_{1-x}Sn_xNi_3$ is still possible due to the entropy contribution.

Table 4. Optimized crystallographic data of Ti_5Sn_3, Ti_5NiSn_3, hypothetical Ni_5NiNi_3, $SnNi_3$, $TiNi_3$, $Ti_{0.5}Sn_{0.5}Ni_3$, $Sn_{0.5}Ti_{0.5}Ni_3$ and Ti_2Sn_3 compounds derived from DFT calculations.

Atom	Wyckoff	x/a	y/b	z/c
Ti_5Sn_3 (a = 0.8102119, c = 0.5453824 nm)				
Ti1	6g	0.242235	0	0.25
Ti2	4d	1/3	2/3	0
Sn1	6g	0.608723	0	0.25
Ti_5NiSn_3 (a = 0.8250848, c = 0.5511669 nm)				
Ti1	6g	0.256722	0	0.25
Ti2	4d	1/3	2/3	0
Sn1	6g	0.610405	0	0.25
Ni1	2b	0	0	0
Ni_5NiNi_3 (a = 0.6970264, c = 0.4840398 nm)				
Ni1	6g	0.333297	0	0.25
Ni2	4d	1/3	2/3	0
Ni3	6g	0.666532	0	0.25
Ni4	2b	0	0	0
$SnNi_3$ (a = 0.535448, c = 0.8647618 nm)				
Sn1	2a	0	0	0
Sn2	2d	1/3	2/3	3/4
Ni1	6g	1/2	0	0
Ni2	6h	0.177094	0.354189	1/4
$TiNi_3$ (a = 0.5137315, c = 0.8382629 nm)				
Ti1	2a	0	0	0
Ti2	2d	1/3	2/3	3/4
Ti_2Sn_3 (a = 0.6013709, b = 2.0176674, c = 0.7073997 nm)				
Ti1	8f	0	0.080577	0.047598
Ti2	8e	1/4	0.33657	1/4
Sn1	8f	0	0.120959	0.426385
Sn2	8f	0	0.224113	0.073991
Sn3	8e	1/4	0.479599	1/4

The calculations were also carried out for the high-pressure modifications (Cu_3Au-type) of $TiNi_3$ and Ni_3Sn binaries and the intermediate composition $Ti_{0.5}Sn_{0.5}Ni_3$. For the intermediate composition the unit cell was doubled in all three directions of the basis vectors (2a×2b×2c) giving in total 32 atoms in the supercell and the symmetry was reduced to $P1$. The optimised values of the lattice parameter a for $TiNi_3$, Ni_3Sn, and $Ti_{0.5}Sn_{0.5}Ni_3$ are 0.36077234, 0.37354910, and 0.367873 nm, respectively. The slope of the $a(x)$ dependence in the range 0≤x≤0.5 is higher than for the higher x values. Most likely this is due to the impact of s- and p-states of Sn atoms that could increase the covalent contribution into the system of chemical bonds.

$(Ti_{1-x}Ni_x)_{1-y}Sn_y$: For the solid solution based on binary TiNi three isotypic structures were modelled: TiNi, TiSn, and NiSn with optimized lattice parameter a = 0.302378757, 0.3430739, and 0.32247303 nm, respectively. The calculated ΔH values of the hypothetical solid solutions between TiNi, TiSn, and NiSn are collected in Table 5. For the intermediate compositions the unit cell was doubled in all three directions of the basis vectors (2a×2b×2c) giving in total 16 atoms in the supercell and the symmetry was reduced to $P1$. The composition $Ti_{0.5}Sn_{0.5}Ni$ is omitted in Table 5 as it corresponds to the $TiNi_2Sn$ compound.

Table 5. DFT values of the enthalpy of formation (ΔH) for selected compounds and their derivatives in the Ti-Ni-Sn system.

Compound	ΔH (meV/atom)	References
TiNiSn	-547.083	This work
	-715	Ref.5
	-549	Ref.7
$TiNi_{1.25}Sn$	-493.933	This work
$TiNi_{1.5}Sn$	-466.162	This work
$TiNi_{1.75}Sn$	-461.613	This work
$TiNi_2Sn$	-472.872	This work
	-622	Ref.5
Ti_2Ni_2Sn	-468.209	This work
	-485	Ref.5
Ti_5NiSn_3	-404.251	This work
	-388	Ref.5
Ti_5Sn_3	-385.435	Ref.5
	-348	This work
Ni_5NiNi_3	+242.338	This work
Ti_2Sn_3	-354.214	This work
$TiNi_3$	-524.463	This work
	-478	Ref.5
$TiNi_3$ (Cu_3Au-type)	-532.018	This work
	-750	Ref.59
	-484 (LMTO-ASA)	Ref.60
	-488 (FP-LMTO)	Ref.60
$SnNi_3$	-219.215	This work
$SnNi_3$ (Cu_3Au-type)	-240.291	This work
$Ti_{0.5}Sn_{0.5}Ni_3$	-341.340	This work
$Ti_{0.5}Sn_{0.5}Ni_3$ (Cu_3Au-type)	-341.886	This work
$Sn_{0.5}Ti_{0.5}Ni_3$	-318.140	This work
TiNi	-390.862	This work
	-411	Ref.5
	-610	Ref.59
	-395 (LMTO-ASA)	Ref.60
	-373 (FP-LMTO)	Ref.60
$Ti_{0.875}Sn_{0.125}Ni$	-364.133	This work
$Ti_{0.75}Sn_{0.25}Ni$	-378.446	This work
$Ti_{0.625}Sn_{0.375}Ni$	-413.794	This work
$Ti_{0.25}Sn_{0.75}Ni$	-185.791	This work
NiSn	-15.954	This work
$Ni_{0.75}Ti_{0.25}Sn$	-106.858	This work
$Ni_{0.5}Ti_{0.5}Sn$	+24.483	This work
$Ni_{0.25}Ti_{0.75}Sn$	-141.487	This work
TiSn	-101.017	This work
$TiSn_{0.75}Ni_{0.25}$	-126.421	This work
$TiSn_{0.5}Ni_{0.5}$	-219.074	This work
$TiSn_{0.25}Ni_{0.75}$	-232.767	This work

$TiNi_{1+x}Sn$: The interstitial solid solution based on the half-Heusler TiNiSn phase (Ti in 4a, Ni in 4c, Sn in 4b) was modelled by reducing the symmetry of the crystal to $P1$ and successively filling of four available voids (4d site) with Ni atoms. According to the calculated ΔH values (Table 5) the formation of limited solid solutions between TiNiSn and $TiNi_2Sn$ at T = 0 K is not possible (Table 5). For Ti_2Sn_3 and Ti_2Ni_2Sn the calculated ΔH values that were used in thermodynamic calculations are collected in Table 5 and the optimised crystallographic data of the Ti_2Sn_3 compound are listed in Table 4. The calculated ΔH values for the selected compounds in Ti-Ni-Sn system using full-potential elk code (GGA-PBE) are mostly in a good agreement with those obtained with pseudopotential VASP code (GGA-PBE) [5], except for TiNiSn and $TiNi_2Sn$ (Table 5). This is strange, as for TiNiSn the ΔH values obtained using the same

VASP code and GGA-PBE approximation by Colinet et al. [7] are comparable with our results (Table 5). The heat of formation values for binary TiNi (Table 5) obtained with FLAPW, pseudopotential [5], LMTO-ASA [60], and FP-LMTO [60] methods are comparable with experimental data collected in Ref. 59, while the value calculated using the semi-empirical tight-binding method [59] significantly differs.

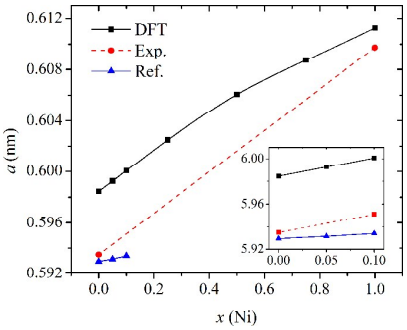

Figure 11. Concentration dependences of optimized (DFT), experimental and reference [5] values of lattice parameter *a* for the $TiNi_{1+x}Sn$ solid solution.

The calculated Δ*H* value for the high-pressure modification of $TiNi_3$ (Table 5) using the FLAPW method is comparable with those obtained by LMTO-ASA and FP-LMTO methods [60], while for the semi-empirical tight-binding method [59] the Δ*H* value is significantly higher. It is interesting to note, that calculations showed higher absolute values of Δ*H* for the high-pressure modifications of $TiNi_3$, Ni_3Sn and intermediate $Ti_{0.5}Sn_{0.5}Ni_3$ in comparison with the normal-pressure modification.

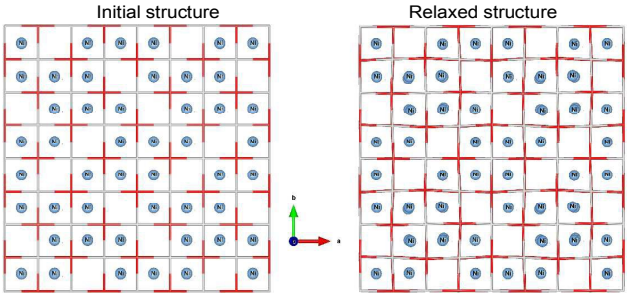

Figure 12. The initial and relaxed geometry of the hypothetical $TiNiSn$-$TiNi_2Sn$ structure.

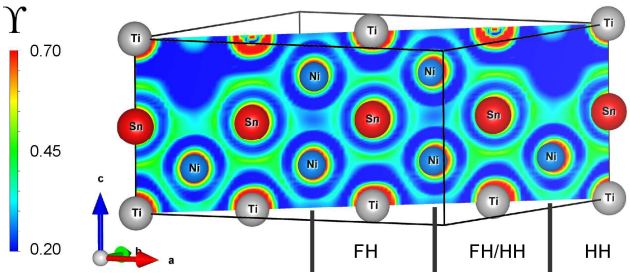

Figure 13. Distribution of the electron localization function along the lattice plane in the $TiNiSn$-$TiNi_2Sn$ structure.

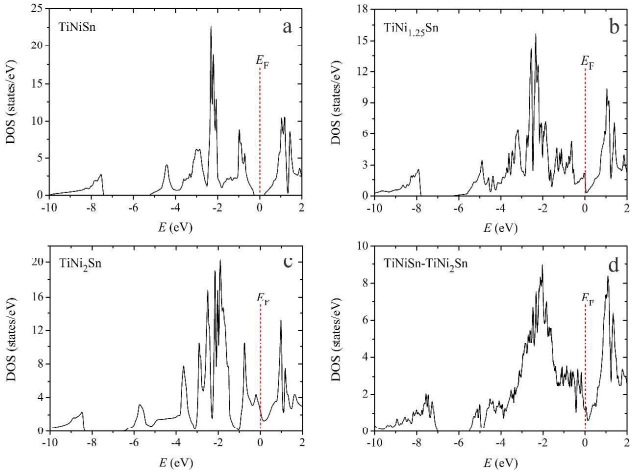

Figure 14. Distribution of the total density of states (per formula unit) for TiNiSn, TiNi1.25Sn, TiNi2Sn, and for the grain boundary TiNiSn-TiNi2Sn. The Fermi level (EF) is at E = 0 eV.

Douglas et al. observed an increase of lattice parameter *a* for the $TiNi_{1+x}Sn$ solid solution in the range $0 \le x \le 0.1$ according to the XRD data [5]. The comparison of optimized (DFT) and experimental values of lattice parameter with a set from Ref. 5 (Fig. 11) shows that the theoretical and interpolated experimental dependencies are almost parallel, while the slope of the reference dependence is more horizontal. Such deviation in slope means that the x(Ni) values corresponding to the lattice parameters in Ref. 5 might be significantly lower. To explain the increase of lattice parameter we have modelled a structure that consists of four TiNiSn unit cells where one Ni atom from each of them diffused to form one full-Heusler $TiNi_2Sn$ unit cell. This is a model of the coherent grain boundary between TiNiSn and $TiNi_2Sn$ phases. The crystal structure geometry optimisation for this model shows that the lattice parameters of TiNiSn and $TiNi_2Sn$ unit cells vary in the ranges 0.58693÷0.58686 and 0.60766÷0.67062 nm, respectively (Fig. 12).

The projection of the electron localization function (Fig. 13) shows localized maxima between Ni and Sn atoms within the half-Heusler (HH) cell and somewhat lower in the full-Heusler (FH) cell. The calculations predict that the presence of the $TiNi_2Sn$ phase strongly affects the TiNiSn lattice parameter value due to the stress on the grain boundary between Heusler and half-Heusler phases. The distribution of the total density of states (Fig. 14) for TiNiSn, $TiNi_{1.25}Sn$, $TiNi_2Sn$, and TiNiSn-$TiNi_2Sn$ grain boundary confirmed that TiNiSn is a semiconductor and $TiNi_2Sn$ is characterized by a metallic type of conductivity. In the case of $TiNi_{1.25}Sn$ (MgAgAs-type) the additional Ni atoms in position 4d generate a new band inside the energy gap and eliminate it. Thus the material predicted has metallic type of conductivity similar to $TiNi_2Sn$. The DOS distribution at the grain boundary of TiNiSn-$TiNi_2Sn$ significantly differs from those in pure TiNiSn and $TiNi_2Sn$. The main difference between TiNiSn and $TiNi_2Sn$ is that the energy bands are strongly delocalised. Like in the case of $TiNi_{1.25}Sn$ and $TiNi_2Sn$ the electrical conductivity at the grain boundary is predicted to be metallic. The deformation of the crystal

structure at the TiNiSn-$TiNi_2Sn$ grain boundary leads to additional phonon scattering and decrease of the thermal conductivity of the material. The increased electrical conductivity and decreased thermal conductivity should have a positive effect on the value of the thermoelectric figure of merit (*Z*).

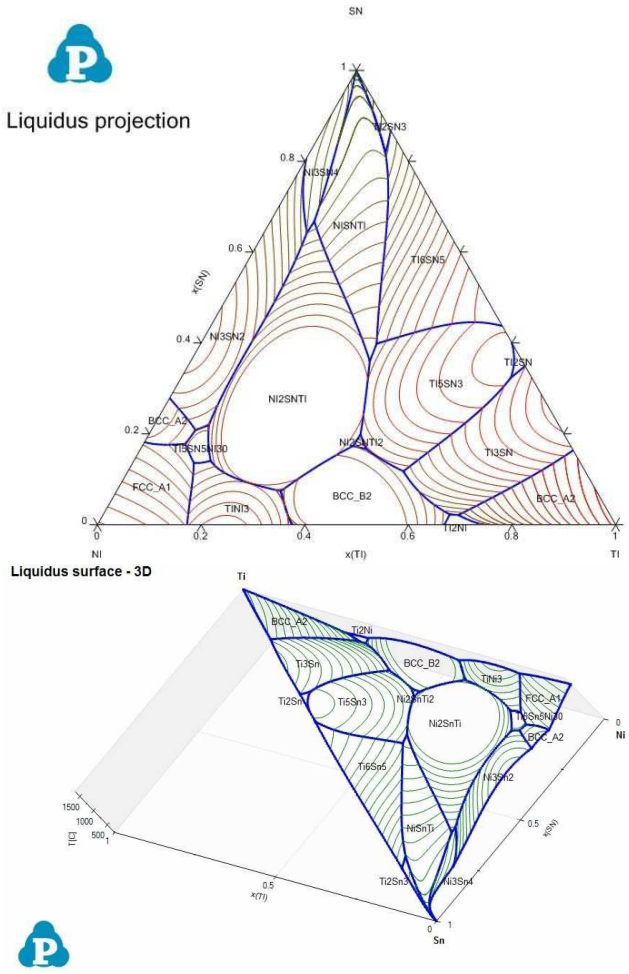

Figure 15. System Ti-Ni-Sn; calculated liquidus projection (top) and 3D view (bottom).

3.4.2.2 Results of Thermodynamic modelling. For thermodynamic modelling of the stability of ternary compounds TiNiSn, $TiNi_2Sn$ and Ti_2Ni_2Sn, the DFT calculated values of the formation energy (ΔH) (Table 5) were used and the entropic term was optimized. Similarly, DFT data were used for Ti_2Sn_3. Data for Ti_5Sn_3 were taken from Ref. 24 and the line solubility to Ti_5NiSn_3 was optimized. The mutual solubility of $TiNi_3$ and $SnNi_3$ was modelled on the basis of binary data from references 23 and 26 and optimized. Stability of TiNi was modelled as B2_BCC and BCC_A2 binary phases [25,26] with optimized solubility of Sn. Note, both phases TiSn and NiSn are in the respective binary systems. The parameters used for the calculations are presented in Table 6. The results of the thermodynamic optimisation are summarized in a liquidus surface (Fig. 15), in a series of isopleths: Ni - TiSn, Sn - TiNi, NiSn - TiSn (Fig. 16), as well as in a series of isothermal sections: 800°C, 900°C, 950°C (Fig. 17), 1050°C and at 1200°C (Fig. 18).

The calculation respects well the experimental melting points Tm of the three ternary compounds: τ_1 (1169 °C calculated /versus 1179 °C experimental), τ_2 (1141 °C /1447 °C), τ_3 (1156 °C /1151°C). Although the overall shape of the liquidus surface is close to the experimental data, several calculated reaction types differ from those experimentally described (for details see the comparison of calculated with experimental reactions given in Table 2). Thus more parameters for liquid and solids may be needed for better consistency between calculation and experiment.

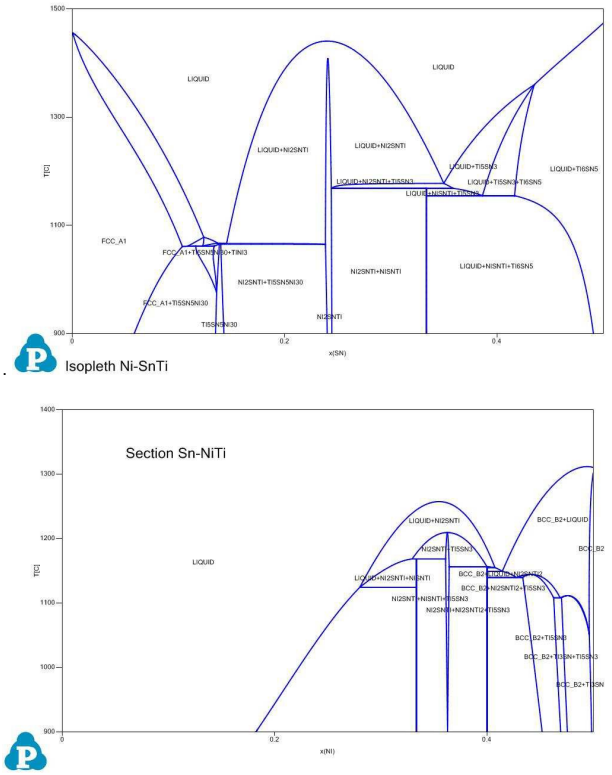

Figure 16. System Ti-Ni-Sn; calculated isopleths Ni-TiSn, Sn-TiNi and NiSn-Ti-Sn.

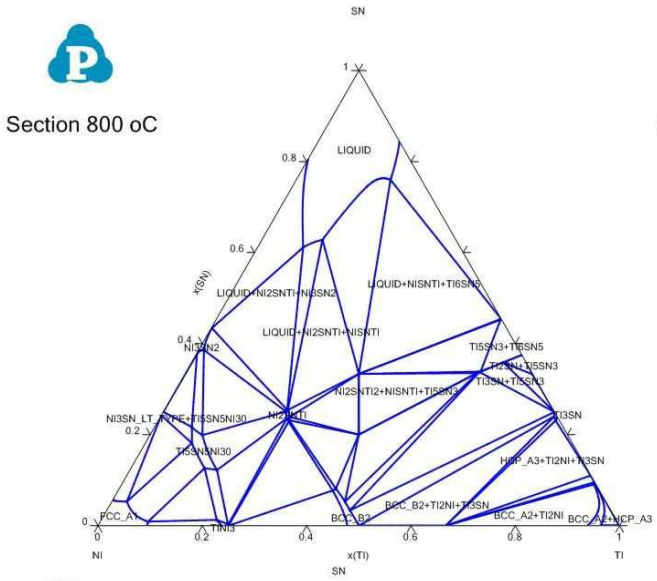

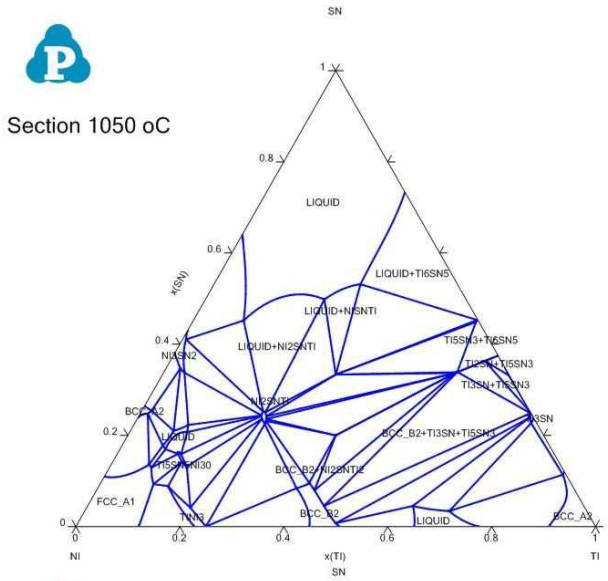

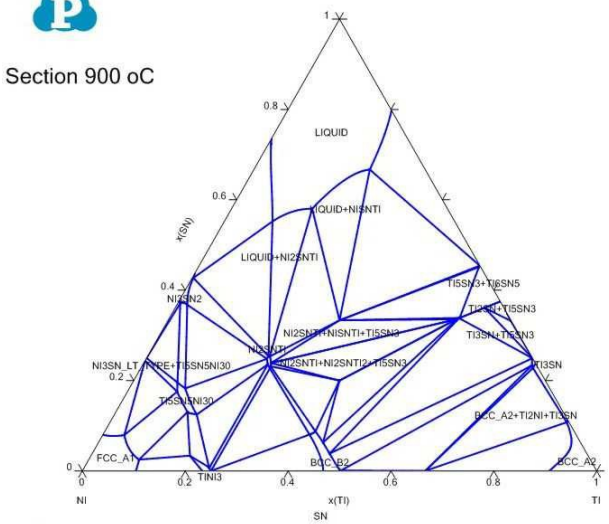

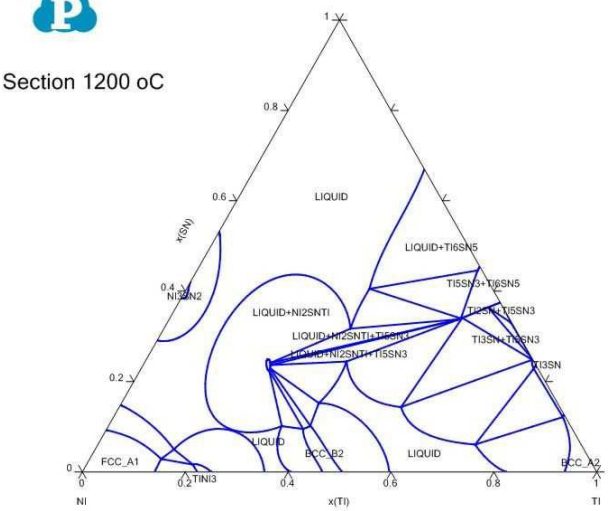

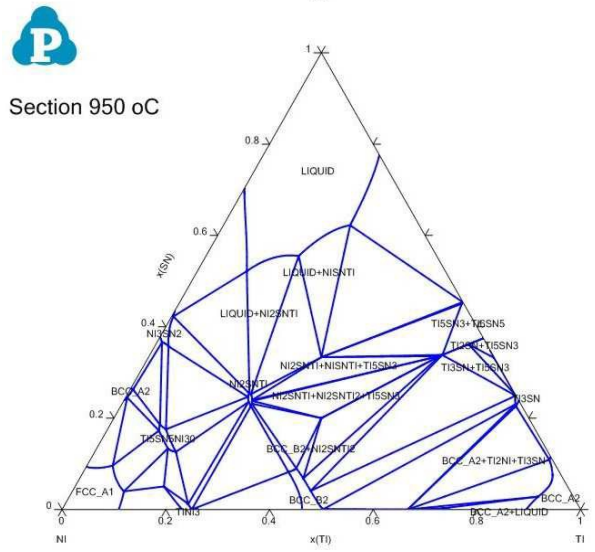

Fig. 17. System Ti-Ni-Sn; calculated isothermal sections at 800, 900 and 950°C.

Fig. 18. System Ti-Ni-Sn; calculated isothermal sections at 1050 and 1200°C.

Table 6. Parameters for calculation of phase equilibria in Ni-Sn-Ti system.

PHASE	Ref.
LIQUID/(Ni,Sn,Ti)	
(0)L(LIQUID,NI,Ti) = -153707.39+34.859449*T	Ref.26
(1)L(LIQUID,NI,TI) = -81824.755+25.809901*T	Ref.26
(2)L(LIQUID,NI,TI) = -10.077897*T	Ref.26
(0)L(LIQUID,SN,TI) = -91598.90-0.9416*T	Ref.24
(1)L(LIQUID,SN,TI) = 45682.64-12.1045*T	Ref.24
(0)L(LIQUID,NI,SN) = -104602.87+197.8089*T-21.6959*T*LN(T)	Ref.23
(1)L(LIQUID,NI,SN) = -30772.17+52.5528*T-7.56094*T*LN(T)	Ref.23
(2)L(LIQUID,NI,SN) = 6582.31	Ref.23
Ternary parameter:	
(0)L(LIQUID,NI,SN,TI) = -10000	[*][a]
Ni3Sn2 / (Ni,Va)1 (Ni,Va)1 (Ni,Sn,Ti)1	
(0)G(NI3SN2,NI:NI:NI) = 31637.299+355.176064*T-66.288*T*LN(T)-0.0145221*T**2	Ref.23
(0)G(NI3SN2,VA:NI:NI) = 21091.532+236.784043*T-44.192*T*LN(T)-0.0098814*T**2	Ref.23
(0)G(NI3SN2,NI:VA:NI) = 21091.532+236.784043*T-44.192*T*LN(T)-0.0098814*T**2	Ref.23
(0)G(NI3SN2,VA:VA:NI) = 10545.766+118.58688*T-22.096*T*LN(T)-0.0048407*T**2	Ref.23
(0)G(NI3SN2,NI:NI:SN;0) = 2*GHSERNI+GHSERSN-83734.818+14.6888165*T	Ref.23
(0)G(NI3SN2,VA:NI:SN) = 5000.+GHSERNI+GHSERSN	Ref.23

PHASE	Ref.
(0)G(NI3SN2,NI:VA:SN) = GHSERNI+GHSERSN-52177.98 +10.774*T	Ref.23
(0)G(NI3SN2,VA:VA:SN) = GHSERSN+20000.0	Ref.23
(0)L(NI3SN2,NI:NI,VA:SN) = -9784.4-12.385*T	Ref.23
(1)L(NI3SN2,NI:NI,VA:SN) = +12000.0	Ref.23
Ternary parameters:	
(0)G(NI3SN2,NI:NI:TI) = GHSERTI+2*GHSERNI-76451.5+3.08647*T]	[*]
(0)G(NI3SN2,VA:NI:TI) = GHSERTI+GHSERNI+123451.5+3.08647*T	[*]
(0)G(NI3SN2,NI:VA:TI) = GHSERTI+GHSERNI-67451.5+3.08647*T	[*]
(0)G(NI3SN2,VA:VA:TI) = GHSERTI+5451.5+3.08647*T	[*]
(0)L(NI3SN2,NI:NI:TI,SN) = -50000	[*]
Ni3Sn4 / (Ni)0.25(Ni,Sn)0.25(Sn)0.5	
(0)G(NI3SN4,NI:NI:SN) = -25078.56+4.291*T+.5*GHSERNI+.5*GHSERSN	Ref.23
(0)G(NI3SN4,NI:SN:SN) = +7613.24+8.749*T+.25*GHSERNI+.75*GHSERSN	Ref.23
(0)L(NI3SN4,NI:NI,SN:SN) = -52928.16	Ref.23
Ni3Sn_LT_TYPE / (Ni,Sn)0.75(Ni,Sn)0.25	
(0)G(NI3SN_LT_TYPE,NI:NI) = +6300.+GHSERNI	Ref.23
(0)G(NI3SN_LT_TYPE,SN:NI) = +5000.+.25*GHSERNI+.75*GHSERSN	Ref.23
(0)G(NI3SN_LT_TYPE,NI:SN) = -28408.+7.0009*T+.75*GHSERNI +.25*GHSERSN	Ref.23
(0)G(NI3SN_LT_TYPE,SN:SN) = +5000.+GHSERSN	Ref.23
FCC_A1 / (Ni,Sn,Ti)1 (Va)1	
(0)L(FCC_A1,NI,TI:VA) = -98143.+6.706*T	Ref.26
(1)L(FCC_A1,NI,TI:VA;1) = -62430	Ref.26
(0)TC(FCC_A1,NI:VA) = +633	Ref.18
(0)BMAGN(FCC_A1,NI:VA) = +0.52	Ref.18
(0)TC(FCC_A1,NI,TI:VA) - -2500	Ref.26
(1)TC(FCC_A1,NI,TI:VA) = -3000;	Ref.26
(2)TC(FCC_A1,NI,TI:VA) = +1300	Ref.26
(0)L(FCC_A1,NI,SN:VA) = -69507.35+74.5697727*T-8.0319551*T*LN(T)	Ref.23
(1)L(FCC_A1,NI,SN:VA) = -12395.19	Ref.23
(0)TC(FCC_A1,NI,SN:VA) = -6000	Ref.22
(1)TC(FCC_A1,NI,SN:VA) = 3000	Ref.22
(0)BMAGN(FCC_A1,NI,SN:VA) - -6.8002	Ref.23
(1)BMAGN(FCC_A1,NI,SN:VA) = 4.3689	Ref.23
Ternary parameter:	
(0)L(FCC_A1,NI,SN,TI:VA) = -170000	[*]
BCC_A2 / (Ni,Ti,Sn,Va)1(Va)3	
(0)L(BCC_A2,NI,TI:VA) = -97427.+12.112*T	Ref.26
(1)L(BCC_A2,NI,TI:VA1) = -32315	Ref.26
(0)TC(BCC_A2,NI,TI:VA) - -575	Ref.26
(0)BMAGN(BCC_A2,NI,TI:VA) = -0.85	Ref.26
(0)L(BCC_A2,NI,SN:VA) = +2369.+43.736*T	Ref.23
(1)L(BCC_A2,NI,SN:VA) = -654762.56+63.272352*T	Ref.23
(2)L(BCC_A2,NI,SN:VA) = +689895.17-94.74087*T	Ref.23
(0)L(BCC_A2,SN,TI:VA) = -142089.52+28.14226*T	Ref.24
(1)L(BCC_A2,SN,TI:VA) = 42811.467	Ref.24
Ternary parameter:	
(0)L(BCC_A2,NI,SN,TI:VA) = +30000	[*]
Disordered part of BCC_B2, identical with BCC_A2	
A2_BCC /(Ni,Ti,Sn)1(Va)3	
(0)L(A2_BCC,NI,TI:VA;0) = -97427+12.112*T	Ref.26
(1)L(A2_BCC,NI,TI:VA) = -32315	Ref.26
(0)TC(A2_BCC,NI,TI:VA) = -575	Ref.26
(0)BMAGN(A2_BCC,NI,TI:VA;0) = -0.85	Ref.26
HCP_A3 /(Ni,Ti,Sn)1(Va)0.5	
(0)L(HCP_A3,NI,TI:VA) = -20000	Ref.26
(0)L(HCP_A3,NI,SN:VA) = 2000	[*]
(0)G(HCP_A3,SN,TI:VA) = -127549.582+23.2048828*T	Ref.24
(1)G(HCP_A3,SN,TI:VA) = 64500.46+7.7566*T	Ref.24
(2)G(HCP_A3,SN,TI:VA) = 31287.55	Ref.24
BCC_B2 / (Ni,Ti,Sn)1(Ni,Ti,Sn)1(Va)3	
(0)G(BCC_B2,NI:TI:VA) = -33193+10.284*T	Ref.26
(0)G(BCC_B2,TI:NI:VA) = -33193+10.284*T	Ref.26
(0)G(BCC_B2,NI:SN:VA) = -40000+11*T	[*]
(0)G(BCC_B2,SN:NI:VA) = -40000+11*T	[*]
(0)G(BCC_B2,TI:SN:VA) = -40000+11*T	[*]
(0)G(BCC_B2,SN:TI:VA) = +40000+11*T	[*]
(0)L(BCC_B2,TI:NI,TI:VA) = +60723.7-15.4024*T	Ref.26
(0)L(BCC_B2,NI,TI:TI:VA) = +60723.7-15.4024*T	Ref.26
(0)L(BCC_B2,NI:NI,TI:VA) = -55288.8+25.4416*T	Ref.26
(0)L(BCC_B2,NI,TI:NI:VA) = -55288.8+25.4416*T	Ref.26
(2)L(BCC_B2,NI:NI,TI:VA) = +6010.11+3.95974*T	Ref.26
(2)L(BCC_B2,NI,TI:NI:VA) = +6010.11+3.95974*T	Ref.26
Ternary parameters:	
(0)L(BCC_B2,TI,SN:NI:VA) = -69000+2*T	Ref.23
(0)L(BCC_B2,NI,SN:NI:VA) = -69000+2*T	Ref.23

PHASE	Ref.
BCT_A5 /(Ni,Sn,Ti)1	
(0)L(BCT_A5,SN,TI) = 50000	Ref.24
(0)L(BCT_A5,NI,SN) = -21500	Ref.23
Ti3Sn / (Ti)3(Ni,Sn,Va)1	
(0)G(TI3SN,TI:SN) = 3*GHSERTI+GHSERSN-141133.07+1.1272*T	Ref.24
(0)G(TI3SN,TI:VA) = 3*GHSERTI+15000	Ref.24
Ternary parameter:	
(0)G(TI3SN,TI:NI;0) = 3*GHSERTI+GHSERNI-45000	[*]
Ti2Sn / (Ti,Va)2(Sn,Ni,Va)1	
(0)G(TI2SN,TI:SN) = 2*GHSERTI+GHSERSN-122344.77+6.0034*T	Ref.24
(0)G(TI2SN,TI:VA) = 2*GHSERTI+10000	Ref.24
(0)G(TI2SN,VA:SN) = GHSERSN+5000	Ref.24
(0)G(TI2SN,VA:VA) 298.15 300000	Ref.24
(0)L(TI2SN,TI:SN,VA) = -34085.17	Ref.24
(0)L(TI2SN,TI,VA:SN) = -49803.91+24.4710*T	Ref.24
Ternary parameters:	
(0)G(TI2SN,VA:NI) = GHSERNI+15000	[*]
(0)G(TI2SN,TI:NI) = 2*GHSERTI+GHSERNI-70000.+6.0034*T	[*]
Ti5Sn3 / (Ti)5(Sn)3(Ni,Va)1	
(0)G(TI5SN3,TI:SN:VA) = 5*GHSERTI+3*GHSERSN-330180+5.3*T	Ref.24
Ternary parameter:	
(0)G(TI5SN3,TI:SN:NI) = 5*GHSERTI+3*GHSERSN+GHSERNI-395000+2.3*T	[*]
Ti6Sn5 / (Ti)6(Ti,Sn,Ni)5	
(0)G(TI6SN5,TI:SN) = 6*GHSERTI+5*GHSERSN-468938.25+5.3729*T	Ref.24
Ternary parameters:	
(0)G(TI6SN5,TI:NI) = 6*GHSERTI+5*GHSERNI-300000.25+5.3729*T	[*]
(0)L(TI6SN5,TI:TI,SN,NI) = 40000	[*]
TiNi3 / (Ni,Ti)1(Ni,Sn,Ti)3	
(0)G(TINI3,NI:NI) = +4*GNIHCP	Ref.25
(0)G(TINI3,NI:TI) = -157744.+18.6544*T+3*GNIHCP+GHSERTI	Ref.26
(0)G(TINI3,TI:NI) = +157744.-18.6544*T+GNIHCP+3*GHSERTI	Ref.26
(0)G(TINI3,TI:TI) = +4*GHSERTI	Ref.25
(0)L(TINI3,NI:NI,TI) = +143216-101.776*T	Ref.26
(1)L(TINI3,NI:NI,TI) = +109156-66.448*T	Ref.26
(0)L(TINI3,TI:NI,TI) = +20000	Ref.26
(0)L(TINI3,NI,TI:TI) = +60000	Ref.26
Ternary parameters:	
(0)G(TINI3,TI:SN) = -100000+GHSERSN+3*GDHCTI	[*]
(0)G(TINI3,NI:SN) = -80000+GHSERSN+3*GDHCNI	[*]
(0)L(TINI3,NI:NI,SN,TI) = -110000	[*]
(0)L(TINI3,TI:NI,SN,TI) = -150000	[*]
Ti2Ni / (Ni,Ti)2(Ni,Ti)1	
(0)G(TI2NI,TI:NI) = +3*GTI2NI	Ref.26
(0)G(TI2NI,NI:TI) = +2*GLAVNI+GLAVTI+30000-3*GTI2NI	Ref.26
(0)L(TI2NI,NI,TI:NI) = +60000	Ref.26
(0)L(TI2NI,NI:NI,TI) = +60000	Ref.26
(0)L(TI2NI,TI:NI,TI) = +60000	Ref.26
(0)L(TI2NI,NI,TI:TI) = +60000	Ref.26
GTI2NI = 0.333333*GHSERNI+0.666667*GHSERTI – 27514.218 +2.85345219*T	Ref.26
Ti2Sn3 /(TI)2(SN)3	
(0)G(TI2SN3,TI:SN)=2*GHSERTI+3*GHSERSN-170900+4.886*T	[*][b]
TERNARY COMPOUNDS:	
NiSnTi / (Ni)1(Sn)1(Ti)1	
(0)G(NISNTI,NI:SN:TI) = +GHSERNI+GHSERTI+GHSERSN-150455+14.2*T	[*][b]
Ni2SnTi2 / (Ni)2(Sn)1(Ti)2	
(0)G(NI2SNTI2,NI:SN:TI) = +2*GHSERNI+2*GHSERTI+GHSERSN-225876+10.51*T	[*][b]
Ni2SnTi / (Ni,Sn,Ti)2(Sn,Va)1(Ti,Va)1	
(0)G(NI2SNTI,NI:SN:TI) = +2*GHSERNI+GHSERTI+GHSERSN-176384+2.83*T	[*][b]
(0)G(NI2SNTI,NI:SN:VA) = +2*GHSERNI+GHSERSN+31200	[*]
(0)G(NI2SNTI,NI:VA:TI) = +2*GHSERNI+GHSERTI+31200	[*]
(0)G(NI2SNTI,NI:VA:VA) = +2*GHSERNI+31200	[*]
(0)L(NI2SNTI,NI:SN:TI,VA) = -49000	[*]
(2)L(NI2SNTI,NI:SN:TI,VA) = -139000	[*]
(0)L(NI2SNTI,NI:SN,VA:TI) = -149000	[*]
Ti5Sn5Ni30 / (Sn,Ti)1(Ni,Va)3	
(0)G(TI5SN5NI30,SN:NI) = 3*GHSERNI+GHSERSN-131928+68.0*T	[*][b]
(0)G(TI5SN5NI30,TI:NI) = 3*GHSERNI+GHSERTI-131928+34.0*T	[*][b]
(0)L(TI5SN5NI30,SN:NI,VA) = -140000	[*]
(0)L(TI5SN5NI30,TI:NI,VA) = -100000	[*]
(0)L(TI5SN5NI30,SN,TI:NI) = -130000	[*]

[*]- this work, [a]optimization, [b] DFT.

Conclusions

From a combined activity of experimental investigation (XPD, EMPA, DTA) and CALPHAD calculation we have established the phase relations in the system Ti-Ni-Sn. The system is characterized by the formation of four ternary compounds labelled τ_1 to τ_4. τ_4-$Ti_{1-x}Sn_xNi_3$ with $AuCu_3$-type exhibits a solution range $0.35 \le x \le 0.73$, A particularly large homogeneity region is recorded for τ_2-$Ti_{1+y}Ni_{2-x}Sn_{1-y}$ (Heusler phase, $MnCu_2Al$-type).

Extended solid solutions starting from binary phases at 950°C have been evaluated for $Ti_5Ni_{1-x}Sn_3$ (filled Mn_5Si_3 = Ti_5Ga_4-type; $0 \le x \le 1$), $Ti_{1-x}Sn_xNi_3$ ($TiNi_3$-type; $0 \le x \le 0.27$) and $(Ti_{1-x}Ni_x)_{1-y}Sn_y$ (CsCl-type) reaching a maximum solubility at x=0.53, y=0.06). From DTA measurements in alumina crucibles under argon a complete liquidus surface has been elucidated revealing congruent melting for τ_2-$TiNi_2Sn$ at 1447°C, but incongruent melting for τ_1-TiNiSn (pseudobinary peritectic formation: $\ell+\tau_2 \leftrightarrow \tau_1$ at 1180°C), τ_3-Ti_2Ni_2Sn (peritectic formation: $L+\tau_2+Ti_5NiSn_3 \leftrightarrow \tau_3$ at 1151°C) and τ_4-$Ti_{1-x}Sn_xNi_3$ (peritectic formation: $L+TiNi_3+(Ni) \leftrightarrow \tau_4$). A Schultz-Scheil diagram for the solidification behavior was constructed for the entire diagram involving 36 isothermal reactions in the ternary.

As for a CALPHAD assessment of the ternary diagram thermodynamic data in the ternary system were only available in the literature for the compounds $TiNi_2Sn$ and TiNiSn, heat of formation data were supplied by our DFT calculations for Ti_2Ni_2Sn, as well as for the solid solutions, which were modelled for $Ti_{1-x}Sn_xNi_3$, $Ti_5Ni_{1-x}Sn_3$ and $(Ti_{1-x}Ni_x)_{1-y}Sn_y$. Thermodynamic calculation was performed with the Pandat software and finally showed a reasonably good agreement for all the 18 invariant reaction isotherms involving the liquid.

Acknowledgements

This research was supported by the Grant Agency of the Czech Republic (Project No. GA14-15576S), by the Project CEITEC-Central European Institute of Technology (CZ.1.05/1.1.00/02.0068) from the European Regional Development Fund and by the Ministry of Education of the Czech Republic (7AMB15AT002).Agency of the Czech Republic (Project No. GA14-15576S), by the Project CEITEC-Central European Institute of Technology (CZ.1.05/1.1.00/02.0068) from the European Regional Development Fund and by the Ministry of Education of the Czech Republic (7AMB15AT002). Part of the research was funded by the Austrian FWF under project P24380. The authors are furthermore grateful to some lattice parameter evaluations made by Philipp Sauerschnig.

References

1 R.V. Skolozdra and Yu.V. Stadnyk, E.E. Starodynova, *Ukr. Fiz. Zh. (Rus. Edition)*, 1986, **31(8)**, 1258.
2 Yu.M. Goryachev, S.V. Kal'chenko, R.V. Skolozdra and Yu.V. Stadnyk, *Elektron. Stroenie i Svoistva Tugoplavk. Soed.,* I Met. AN USSR. In-t Probl. Materialoved., Kiev 1991, 81.
3 G. Schierning, R. Chavez, R. Schmechel, B. Balke, G. Rogl and P. Rogl, *Trans. Mat. Res*., 2015. in press
4 V.V. Romaka, P. Rogl, L. Romaka, Yu. Stadnyk, N. Melnychenko, A. Grytsiv, M. Falmbigl and N. Skryabina, *J. Solid State Chem.*, 2013, **197**, 103.
5 J.E. Douglas, C.S. Birkel, N. Verma, V.M. Miller, Mao-Sheng Miao, G.D. Stucky, T.M. Pollock and R. Seshadri, *J. App.Phys.*, 2014, **115**, 043720.
6 D.-Y. Jung, K. Kurosaki, C.-E. Kim, H. Muta and S. Yamanaka, *J. Alloys Compds.,* 2010, **489**, 328.
7 C. Colinet, P. Jund and J-C. Tédenac, *Intermetallics*, 2014, **46**, 103.
8 M. Yin and P. Nash, Data presented at CALPHAD XLIII. Changsha. Hunan. China. June 1st to June 6th. 2014
9 R.A. Downie, D.A. MacLaren, R.I. Smith and J.W.G. Bos, *Chem. Commun.*, 2013, **49**, 4184.
10 H. Hazama, M. Matsubara, R. Asahi and T. Takeuchi, *J. Appl. Phys.*, 2011, **110**, 063710.
11 J. Rodriguez-Carvajal, FULLPROF, a program for Rietveld refinement and pattern matching analysis, Abstract of the satellite meeting on powder diffraction of the XV congress, p. 127, Int. Union of Crystallography, Talence, France, 1990; see also *Physica B.*, 1993, **55**, 192.
12 W. Wacha, Program STRUKTUR, Master thesis, University of Technology Vienna, 1989.
13 G.M. Sheldrick, *Acta Crystallogr. A*, 1990, **A46**, 467.
14 ELK, Program package; http://elk.sourceforge.net/
15 J.P. Perdew, K. Burke and M. Ernzerhof, *Phys. Rev. Lett*., 1996, **77**, 3865.
16 Pandat software, version 2014, CompuTherm LLC, Madison, Wisconsin, USA, http://www.computherm.com/
17 H.L. Lukas, S.G. Fries and B. Sundman, Computational Thermodynamics, Cambridge Univ. Press, Cambridge, 2007.
18 A.T. Dinsdale, *CALPHAD*, 1991, **15**, 317.
19 O. Redlich and A. Kister, *Industrial & Engineering Chemistry Research,* 1948, **40**, 345.
20 Y.M. Muggianu, M. Gambino and J.P. Bros, *J. Chim. Phys. Phys.-Chim. Biol.,* 1975, **72**, 83.
21 Binary Alloy Phase Diagrams–Second edition, T. B. Massalski, Editor-in-Chief; H. Okamoto, P. R. Subramanian, L. Kacprzak, Editors. ASM International, Materials Park, Ohio, USA. December 1990. xxii, 3589 pp
22 H.S. Liu, J. Wang and Z.P. Jin, *CALPHAD*, 2004, **28**. 363.
23 Zemanova, A. Kroupa and A. Dinsdale, *Monatsh. Chem*. 2012, **143**, 1255.
24 F. Yin, J.-C. Tedenac and F. Gascoin, *CALPHAD*, 2007, **31(3)**, 370.
25 P.Bellen, K.C.Hari Kumar and P.Wollants, *Z.Metallkd*. 1996, **87**, 12.
26 J. De Keyzer, G. Cacciamani, N. Dupin and P. Wollants, *CALPHAD*, 2009, **33**, 109.
27 E. Povoden-Karadeniz, D.C. Cirstea, P. Lang, T. Wojcik and E. Kozeschnik, *CALPHAD,*2013, **41**, 128.
28 F. C. Cannon, *Mater. Res. Soc. Symp. Proc.*, 1984, **22**, 113.
29 P. Pietrokowsky and E.P. Frink, *Trans. Am. Soc, Met.*, 1957, **49**, 339.
30 H. Nowotny, H. Auer Welsbach, J. Bruss and A. Kohl, *Monatsh. Chem.*, 1959, **90**, 15.
31 J.C. Schuster, M. Naka and T. Shibayanagi, *J. Alloys Compd.*, 2000, **305**, L1.
32 K. Schubert, K. Frank and R. Gohle, *Naturwissenschaften*, 1963, **50**, 41.
33 J. H. N. Van Vucht, H.A.C.M. Bruning, H.C. Donkerloot and A.H. Gomes de Mesquita, *Philips Res. Rep.*, 1964, **19**, 407
34 H. Kleinke, M. Waldeck and P. Gütlich, *Chem. Mater.*, 2000, **12**, 2219.
35 S. Sridharan, H. Nowotny and S. F. Wayne, *Monatsh. Chem.*, 1983, **114**, 127.

36 E. L. Semenova and Yu.V. Kudryavtsev, *J. Alloys Compds.,* 1994, **203**, 165.
37 W. Buhrer, R. Gotthardt, A. Kulik, O. Mercier and F.Staub, *J. Phys. F: Met. Physh.*, 1983, **13**, L77.
38 J.L. Glimois, P. Forey, R. Guillen and J.L. Feron, *J. Less Common Met.*, 1987, **134**, 221.
39 M. Wilkens, J. Wegst, E. Gunzel, W. Burkhardt, H.G. Meissner, W. Schutt, K. Schubert and P. Esslinger, *Naturwissenschaften*, 1956, **43**, 248.
40 S. K. Shadangi, M. Sing, S. C. Panda and S. Bhan, *Cryst. Res. Technol.*, 1986, **21**, 867.
41 H. Fjellvag and A. Kjekshus, *Acta Chem. Scand., A: Phys. Inorg. Chem.*, 1986, **40**, 23.
42 W. Jeitschko and B. Jaberg, *Acta Crystallogr., Sec. B*, 1982, **38**, 598.
43 M.K. Bhargava, K. Schubert, *J. Less Common Met.*, 1973, **33**, 181.
44 V. A. Romaka, Yu. V. Stadnyk, D. Fruchart, T. I. Dominuk, L. P. Romaka, P. Rogl and A. M. Goryn, Semiconductors, 2009, **43**, 1124.
45 H.P. Stüwe, Y. Shimomura, *Z. Metallkd.*, 1960, **51**, 180.
46 G.R. Purdy and J.G. Parr, *Trans. Am. Inst. Min. Metall. Pet. Eng.*, 1961, **221**, 636.
47 P. Duwez and J.L. Taylor, *Trans. Am. Inst. Min. Metall. Pet. Eng.*, 1950, **188**, 1173.
48 D.M. Poole and W. Hume Rothery, *J. Inst. Met.*, 1954/55, **83**, 473.
49 Taylor and R.W. Floyd, *J. Inst. Met.*, 1951/52, **80** , 577-587.
50 T. V. Philip and P.A. Beck, *Trans. Am. Inst. Min. Metall. Pet. Eng.*, 1957, **209**, 1269.
51 F.J.J. Van Loo, G.F. Bastin and A.J.H. Leenen, *J. Less Common Met.*, 1978, **57**, 111.
52 Shinogi, M. Tanaka and K. Endo, *J. Phys. Soc. Jpn.*, 1978, **44**, 774.
53 E.A. Görlich, K. Latka, A. Szytula, D. Wagner, R. Kmiec and K. Ruebenbauer, *Solid State Commun.*, 1978, **25**, 661.
54 W. Jeitschko , *Metall. Trans.*, 1970, **1(11)**, 3159.
55 J. Pierre, R.V. Skolozdra and Y.V. Stadnyk, *J. Magn. Magn. Mater.*, 1993, **128**, 93.
56 P.G Van Engen, K.H.J. Buschow and M. Erman, *J. Magn. Magn. Mater.*, 1983, **30**, 374.
57 H. Hazama, M. Matsubara, R. Asahi and T. Takeuchi, *J. Appl. Phys.*, 2011, **110**, 063710.
58 E. Parthé, L. Gelato, B. Chabot, M. Penzo, K. Cenzual and R. Gladyshevskii, TYPIX Standardized Data and Crystal Chemical Characterization of Inorganic Structure Types, Berlin, Germany, Springer, 1994.
59 P. Mikušik and Š. Pick, *Solid State Communications*, 1993, **86(7)**, 467.
60 Pasturel, C. Colinet, D. Nguyen Manh, A.T. Paxton and M. van Schilfgaarde, *Phys. Rev. B.*, 1995, **52(21)**, 15176.